Alternative ergosterol biosynthetic pathways confer antifungal drug resistance in the human pathogens within the *Mucor* species complex

María Isabel Navarro-Mendoza[1,4,✉], Carlos Pérez-Arques[1,4,✉], Josie Parker[2], Steven Kelly[3], and Joseph Heitman[1,✉]

[1]Department of Molecular Genetics and Microbiology, Duke University School of Medicine, NC 27710, USA
[2]Molecular Biosciences Division, School of Biosciences, Cardiff University, Cardiff, Wales, UK
[3]Institute of Life Science, Swansea University Medical School, Swansea, Wales, UK
[4]Authors contributed equally

Abstract

Mucormycoses are emerging fungal infections caused by a variety of heterogeneous species within the order Mucorales. Among the *Mucor* species complex, *Mucor circinelloides* is the most frequently isolated pathogen in mucormycosis patients and despite its clinical significance, there is an absence of established genome manipulation techniques to conduct molecular pathogenesis studies. In this study, we generated a spontaneous uracil auxotrophic strain and developed a genetic transformation procedure to analyze molecular mechanisms conferring antifungal drug resistance. With this new model, phenotypic analyses of gene deletion mutants were conducted to define Erg3 and Erg6a as key biosynthetic enzymes in the *M. circinelloides* ergosterol pathway. Erg3 is a C-5 sterol desaturase involved in growth, sporulation, virulence, and azole susceptibility. In other fungal pathogens, *erg3* mutations confer azole resistance because Erg3 catalyzes the production of a toxic diol upon azole exposure. Surprisingly, *M. circinelloides* produces only trace amounts of this toxic diol and yet, it is still susceptible to posaconazole and isavuconazole due to alterations in membrane sterol composition. These alterations are severely aggravated by *erg3*Δ mutations, resulting in ergosterol depletion and consequently, hypersensitivity to azoles. We also identified Erg6a as the main C-24 sterol methyltransferase, whose activity may be partially rescued by the paralogs Erg6b and Erg6c. Loss of Erg6a function diverts ergosterol synthesis to the production of cholesta-type sterols, resulting in resistance to amphotericin B. Our findings suggest that mutations or epimutations causing loss of Erg6 function may arise during human infections, resulting in antifungal drug resistance to first-line treatments against mucormycoses.

Importance

The *Mucor* species complex includes a variety of opportunistic pathogens known to cause mucormycosis, a potentially lethal fungal infection with limited therapeutic options. The only effective first-line treatments against mucormycosis consist of liposomal formulations of amphotericin B and the triazoles posaconazole and isavuconazole, all of which target components within the ergosterol biosynthetic pathway. This study uncovered *M. circinelloides* Erg3 and Erg6a as key enzymes to produce ergosterol, a vital constituent of fungal membranes. Absence of any of those enzymes leads to decreased ergosterol and consequently, resistance to ergosterol-binding polyenes such as amphotericin B. Particularly, losing Erg6a function pose a higher threat as the ergosterol pathway is channeled into alternative sterols similar to cholesterol, which maintain membrane permeability. As a result, *erg6a* mutants survive within the host and disseminate the infection, indicating that Erg6a deficiency may arise during human infections and confer resistance to the most effective treatment against mucormycoses.

Genetic transformation | ergosterol | antifungal drug resistance | Erg3 | Erg6 | Mucorales | fungal pathogens

Correspondence: ***heitm001@duke.edu, maribel.navarro@duke.edu, carlos.parq@duke.edu***

Introduction

Mucorales comprise an order of filamentous fungi that includes *Mucor*, *Rhizopus*, and *Lichtheimia* human pathogenic species. These species cause infections known as mucormycoses, which typically occur when individuals inhale the spores of these molds or are infected through skin injuries, burns, or other traumatic wounds (1). Immunocompromised patients, such as those with cancer and/or undergoing immunosuppressive treatment, are particularly susceptible to invasive mucormycoses. Individuals suffering from poorly controlled diabetes mellitus are also at higher risk. This disease is associated with poor prognoses and dramatically high morbidity, resulting in mortality rates ranging from 23 % to 80 % (2). Because Mucorales are understudied pathogens, it is challenging to gather information on global incidence rates. Nevertheless, the trend over the past decade has shown an increase in the number of cases, especially associated with COVID-19 infections (3, 4), which has led the World Health Organization to include mucoralean pathogens on their fungal priority pathogens list (5).

Recent global practice guidelines discourage the use of fluconazole, voriconazole (6), or the echinocandins (7) as therapeutic options for mucormycoses due to inherent resistance to those antifungal drugs. Instead, first-line treatment with liposomal formulations of the polyene amphotericin B is recommended at high doses, followed by salvage treatment with the triazoles posaconazole or isavuconazole (2). However, the applicability of these treatments can be limited by toxicity and resistance. Due to the limited availability of effective antifungal drugs, the emergence of resistant strains in the environment or in the host poses a global threat to pub-

lic health. Antifungal drug resistance mechanisms in mucoralean clinical isolates are poorly understood, due to the lack of proper diagnostic tools and the heterogeneity of infections (5). Recent studies have revealed gain-of-function mutations in *erg11* confer resistance to azoles (6). Additionally, a novel mechanism for antifungal drug resistance based on RNA interference (RNAi), called epimutation, has been discovered in *Mucor* species (8). This mechanism could represent a source of transient antifungal drug resistance during host infection (9). The epimutation mechanism operates through RNAi-mediated gene silencing, repressing the expression of drug targets. Therefore, identifying loss-of-function mutations conferring antifungal drug resistance might elucidate new targets of this epigenetic process.

Understanding the mechanisms of action of the recommended antifungal therapies against mucormycoses may help to identify drug targets involved in drug resistance. Polyenes bind directly to ergosterol and both increase membrane permeability and sequester ergosterol (10, 11), while azoles block the main ergosterol biosynthetic pathway by inhibiting the Erg11 enzyme (12). By antagonistically binding Erg11, azoles can divert ergosterol biosynthesis into a different pathway that results in toxic sterol intermediates (13, 14). Thus, the mechanisms of action of both polyenes and azoles converge on ergosterol production and conceivably, altering the ergosterol biosynthetic pathway may lead to changes in drug susceptibility. Indeed, loss-of-function mutations in two key ergosterol biosynthetic genes, *erg3* and *erg6*, have been reported to result in antifungal drug resistance in other fungal pathogens. Erg3 is a C-5 sterol desaturase involved in the main ergosterol pathway, but also in the toxic sterol pathway (13). Therefore, loss of Erg3 function prevents the formation of toxic sterol intermediates produced during azole treatment, enabling evasion of the fungistatic effect of the drug (14, 15). Clinical isolates of *Candida* species, including *Candida albicans*, *Candida parapsilosis*, *Candida glabrata,* and *Candida lusitaniae*, are rendered resistant to azoles via mutations in the *erg3* gene, with some exhibiting cross-resistance to amphotericin B (13, 16–20). On the other hand, Erg6 is a C-24 sterol methyltransferase that either converts zymosterol into fecosterol or lanosterol into eburicol (21), two alternative ergosterol precursors. Mutations affecting Erg6 function favor the production of cholesta-type sterols, conferring polyene resistance in several fungal pathogens, including *C. albicans* (22), *Candida auris* (23), *C. lusitaniae* (24), *C. glabrata* (25), and *Cryptococcus neoformans* (26, 27). Moreover, *erg6* mutations have been characterized in clinical isolates in *C. glabrata* and *C. auris*. Notably, these mutations arise inside the host during polyene therapy, thus contributing to the global emergence of antimicrobial drug resistance (23, 28). Research on molecular mechanisms leading to drug resistance in Mucorales is of paramount importance, albeit challenging given current genetic and molecular models and tools.

Mucor is a genus of related fungal species within the order Mucorales. Previously, the *Mucor circinelloides* species complex was delineated into *formae* but recent taxonomic and phylogenetic analyses have defined a minimum of 16 distinct phylogenetic species, 7 of which are known to cause human disease (29). *M. circinelloides* is the *Mucor* species most frequently isolated from clinical sources and is associated with mucormycotic infections (30–32). As a consequence, research has advanced genetics, genomics, and host-microbe interaction models for this understudied group of pathogens, leading to the development of *Mucor* as a model for mucormycoses over the past decade (8, 33–36). All of these studies relied on *M. lusitanicus* because it was the only species amenable to genetic transformation and it has a well assembled genome available (37, 38). Yet among *Mucor* species, *M. lusitanicus* is not a frequent cause of mucormycosis, probably due to its maximum growth temperature being 35 to 37 °C, compared to *M. circinelloides,* which grows at 37 to 39 °C (29). In this study, we introduce a new model to study mucormycosis pathogenesis and antifungal drug susceptibility in *M. circinelloides*. We developed a novel transformation method to characterize the *erg3* and *erg6* genes in a *M. circinelloides* pathogenic isolate, leading to the discovery of new mechanisms for amphotericin B resistance and azole susceptibility in the Mucorales.

Results

A genetic transformation procedure for *Mucor circinelloides* pathogenic species. *M. circinelloides* is the most frequent *Mucor* species isolated from mucormycosis patients, and these isolates are usually thermotolerant and highly virulent in host-pathogen infection models, yet reliable genetic transformation procedures are not available for this species. To develop a genetic model for virulence and antifungal susceptibility studies, we aimed at generating a *M. circinelloides* strain that is competent for genetic transformation. Because ensuring full virulence and thermotolerance in our model was a priority, *M. circinelloides* 1006PhL human isolate (hereinafter *M. circinelloides*) was selected to conduct studies as it has both attributes (39). Also, its genome has been sequenced (40) and is publicly available (https://www.ncbi.nlm.nih.gov/datasets/genome/GCA_000401635.1/), providing a critical advantage to design integrative DNA cassettes, which rely on homologous recombination repair mechanisms. Traditionally in mucoralean genetics, the application of dominant resistance markers is not possible due to high intrinsic resistance to these drugs. Because *M. circinelloides* had not been specifically tested, it was cultured with drugs frequently utilized for transformant selection. Even at high concentrations, *M. circinelloides* exhibits residual growth on the plates, complicating the discrimination between resistant transformants and residually growing colonies (Figure S1).

As a consequence, we designed a workflow to obtain an auxotrophic mutant that could serve as a transformation recipient strain, a method that proved effective in genetically transforming Mucorales in previous studies (41). 5-fluoroorotic acid (5-FOA) is sequentially converted into a cytotoxic metabolite known as 5-fluorouracil (5-FU), by the action of the orotate phosphoribosyltransferase PyrF

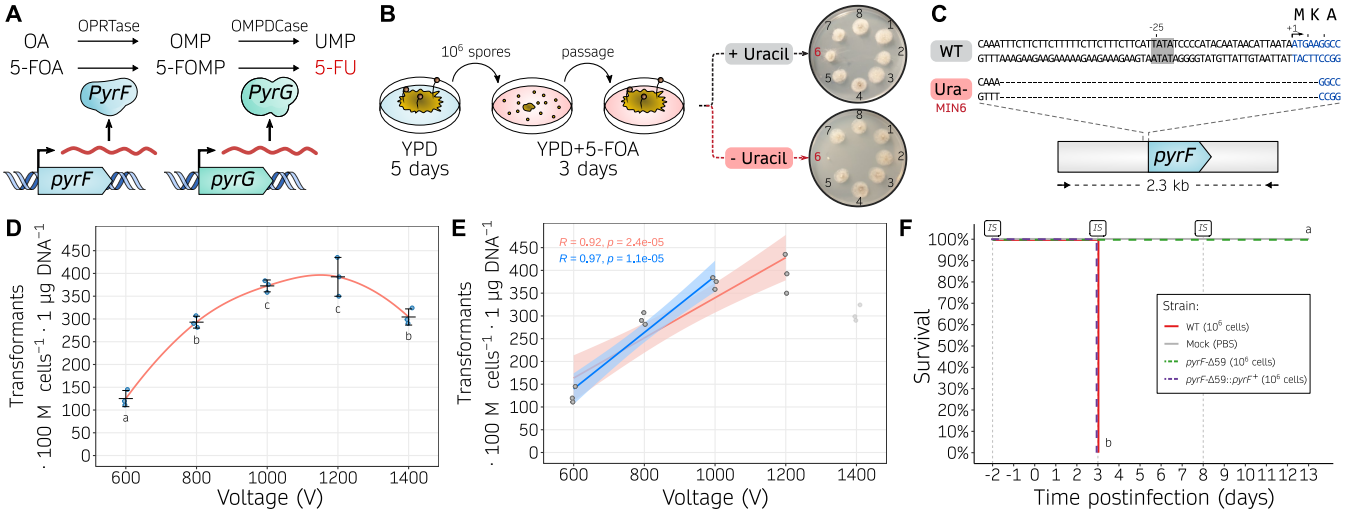

Figure 1. Uracil auxotrophy enables *M. circinelloides* transformation based on a *pyrF* selectable marker. (A) Role of PyrF (orotate phosphoribosyltransferase, OPRTase) and PyrG (orotidine monophosphate decarboxylase, OMPDCase) in the uracil biosynthetic pathway, converting orotic acid (OA) to orotidine monophosphate (OMP), and OMP into uridine monophosphate (UMP), respectively. Alternatively, the same enzymes catalyze the conversion of 5-fluoroorotic acid (5-FOA) into fluoro-OMP (FOMP), and FOMP into 5-fluorouracil (5-FU), respectively. **(B)** Experimental design followed to isolate uracil auxotrophic strains. Briefly, wildtype spores were collected from YPD medium, counted, and one million spores were plated onto YPD containing 5-FOA. After three days, 5-FOA resistant colonies were isolated and transferred to new 5-FOA containing medium to confirm the resistance, and then inoculated onto minimal medium either with or without uracil to confirm the auxotrophy. **(C)** *pyrF* sequences from the wildtype and uracil auxotrophic strains (Ura-, MIN6), focusing on the 5'-region of the gene. The TATA box motif (gray background around position -25), transcription start site (arrow, position +1), *pyrF* coding sequence (blue font), and encoded one-letter amino acids are shown. **(D, E)** Transformation efficiency measured as transformants per 100 million protoplasts per microgram of DNA using different voltages in the electroporation procedure. Individual values (dots) from biological triplicates were used to determine the mean and SD values as black lines. In **(D)**, a smoothed curve is drawn as a red line. Significant differences among voltages were determined by a One-way ANOVA and Tukey HSD test, and voltages showing different letters indicate significant differences (*p-value* $\leq$ 0.05). In **(E)**, two linear regression models are displayed showing a positive correlation for voltages from 600 to 1,000 V (blue line) or to 1,200 V (red line). Pearson's correlation coefficients (R) are shown for each regression. **(F)** Kaplan-Meier survival curves of immunosuppressed mice after infection with *M. circinelloides* wildtype and transformable strains (color-coded). Intraperitoneal immunosuppressive (IS) treatments are shown. Strains showing significant differences in virulence are indicated as different letters (*p-value* $\leq$ 0.0001), assessed by a Log-rank test.

and the orotidine-5'-monophosphate decarboxylase PyrG. As these two enzymes also catalyze essential steps in the uracil biosynthetic pathway, loss-of-function mutations in any of their encoding genes results in resistance to 5-FOA and uracil auxotrophy that can be rescued by uridine and/or uracil supplementation. Following this rationale (Figure 1A), we selected for spontaneous uracil auxotrophic mutants by culturing spores in the presence of 5-FOA but avoiding additional mutagenic agents to prevent undesired secondary mutations. A total of 237 5-FOA resistant colonies were isolated and 8 were tested for uracil auxotrophy by comparing their ability to grow on media with or without uridine and uracil. Among these, one isolate named MIN6 was unable to grow without uridine and uracil indicative of uracil auxotrophy (Figure 1B, isolate 6). Subsequent Sanger-sequencing of the *pyrF* and *pyrG* genes revealed a 59-basepair (bp) microdeletion within the *pyrF* locus (*pyrF*-Δ59). This microdeletion comprises the last 54 bp of the promoter region, including a putative TATA-box element whose deletion may impair transcription; and the first 5 bp of the coding sequence, leading to a start loss and a consequent frameshift mutation assuming translation would start at the next available AUG triplet (Figure 1C).

Next, we attempted to complement MIN6 uracil auxotrophy by integrating the *pyrF* marker, a 2.3-kilobase (kb) DNA fragment comprising the wildtype *pyrF* promoter, coding sequence, and terminator regions aiming at favoring homologous recombination and subsequent replacement of the *pyrF*-Δ59 allele with its wildtype sequence. To integrate the *pyrF* marker, we improved a reliable protoplast transformation procedure involving electroporation. For optimal protoplast preparation, the spore germination rate in *M. circinelloides* was comparatively slower than in *M. lusitanicus*; this delay may be attributed to the pre-swollen and larger size of *M. lusitanicus* spores (42). DNA was introduced into the protoplasts by exponential decay waveform electroporation with constant capacitance and resistance, and transformation efficiency was assessed at different voltages to select the optimum for subsequent gene replacement experiments (Figure 1D). The most efficient transformation rate was obtained with 1200 V, although there were not significant differences between 1000 and 1200 V. A linear regression modeling indicates a positive correlation between transformation efficiency and voltage, particularly significant at voltages ranging from 600 to 1000 V (Figure 1E). Therefore, subsequent electroporations were conducted at 1000 V to ensure maximum efficiency while avoiding unnecessary protoplast lethality. The successful complementation of the *pyrF*-Δ59 allele through homologous recombination with a wildtype *pyrF* marker as a donor template was verified by PCR-amplification and restriction fragment length polymorphism (RFLP, Figure S2).

Because one of our aims was to provide a robust genetic model to drive research in mucormycosis pathogenesis, we determined the effect of the *pyrF*-Δ59 allele on virulence and tested whether *pyrF* complementation could rescue a fully virulent phenotype (Figure 1F). To do so, the virulence potential of the wildtype 1006PhL strain, the *pyrF*-Δ59 uracil auxotrophic strain, and the *pyrF*-Δ59::*pyrF*$^+$ complemented

strain were analyzed in a survival assay using immunosuppressed mice. The uracil auxotrophic strain showed a complete and significant lack of virulence, whereas all of the mice challenged with the wildtype 1006PhL or *pyrF*$^+$ complemented strain succumbed to the infection and displayed identical survival curves without significant differences. Similarly, animals infected with the uracil auxotroph displayed a weight increment curve similar to animals infected with only PBS as a mock control, as opposed to the acute weight loss exhibited by animals infected with the wildtype or complemented strains (Figure S3). These results demonstrate that uracil auxotrophy impairs the pathogenic potential of *M. circinicelloides*, and shows that full virulence can be restored by *pyrF*$^+$ complementation through genetic transformation. Overall, these findings highlight this procedure as a highly efficient, reliable method to obtain uracil auxotrophic strains, transform by electroporation, and replace genes by homologous recombination in *M. circinelloides*. But more importantly, they support the application of this genetic model to study virulence processes and antimicrobial drug resistance within the *Mucor* species complex, as opposed to other thermosensitive, partially virulent, and clinically less relevant species such as *M. lusitanicus*.

Erg3 and Erg6 distribution across the Mucoromycota. Because antifungal drugs often target essential components of the fungal cell wall, mutations in the ergosterol biosynthetic pathway –the principal sterol found in the membranes of most terrestrial fungi– can lead to antifungal drug resistance. For instance, *erg3* and *erg6* loss-of-function mutations have been shown to alter susceptibility to polyene and azole drugs, and also to impact the virulence potential of several fungal pathogens (43, 44). As a proof of concept, we aimed to delete the *erg3* and *erg6* genes in *M. circinelloides* and *M. lusitanicus* to illustrate the potential of our newly transformable *M. circinelloides* strain for standardized antifungal susceptibility testing and virulence assays. A protein-protein similarity search identified one Erg3 and three Erg6 homologs whose evolutionary history was examined by phylogenetic tree inference using representative protein sequences from several pathogenic species from the Mucoromycota, as well as from model organisms with single-copy *erg* genes for reference (Figure 2, Tables S1 for Erg3, and Tables S2 for Erg6 sequences). Erg3 protein sequences from Mucoromycota fungi form a robust clade within fungal Erg3 proteins, highly consistent with their species phylogeny (Figure 2A). This phylogeny suggests two independent duplication events in the Lichtheimiaceae and Rhizopodaceae families as most of their members harbor two Erg3 paralogs, which could be explained by recent segmental duplication events in these families (45–47). Besides these exceptional duplication events, most Mucoromycota species harbor a single Erg3 ortholog and particularly, the clade comprising *Mucor* species. The Erg3 ortholog exhibits high synteny among *Mucor* species (Figure 2C and Figure S4A), confirming our phylogenetic inference. In addition, RNA-sequencing and transcriptomic analysis revealed that *erg3* is transcribed in both *Mucor* species and allowed us to manually curate the untranslated regions. Taken together, these results indicate that *erg3* deletion will suffice to confer loss of Erg3 function.

On the other hand, the evolutionary history of Erg6 is more complex (Figure 2B). We identified a robustly supported, monophyletic clade encompassing the orthologs from well-known model organisms as well as Glomeromycota and Mucoromycota Erg6 paralogs. This clade exhibits two different Erg6 paralogs from *Mucor* species: one closer to the clade root and the reference Erg6 sequences (Figure 2B, Erg6a) and another considerably divergent (Figure 2B, Erg6c, bottom clade). In addition, *Mucor* species harbor another Erg6 paralog, that is more divergent compared to the reference Erg6 sequences (Figure 2B, Erg6b). To provide a further analysis on the origin of these paralogs, we developed a model (Figure 2E) that offers the most plausible interpretation of the phylogenetic and synteny patterns observed across all of the Mucoromycota species analyzed (Figure S4D-H). First, there was an ancient duplication event predating the Glomeromycota and Mucoromycota common ancestor, as species from both phyla harbor at least two extremely divergent Erg6 paralogs (Figure 2B, EDF duplication, *Rhizophagus irregularis* and the Mucoromycota). This was followed by another duplication event coinciding with a previously reported whole-genome duplication that occurred in the mucoralean common ancestor (37). Subsequent gene loss in many lineages resulted in most Mucoromycota harboring two to three Erg6 paralogs that started to diverge close to the last mucoralean common ancestor. Interestingly, gene loss did not occur uniformly in all species or genera: e.g., the third paralog found in *Mucor* species (Erg6c) is different from that of *Lichtheimia* species (Erg6d), and several species harbor only two paralogs (Erg6a and Erg6b). Moreover, Rhizopodiaceae species exhibit an additional, more recent duplication (Erg6e), which is consistent with another round of whole-genome duplication and subsequent gene loss in this lineage (46, 47). All three Erg6 paralogs found in *Mucor* species, which also show conserved synteny (Figure 2D, Figure S4D-H), are explained by this model. Interestingly, RNA-sequencing and transcriptomic analysis revealed that only *erg6a* is actively expressed (Figure 2D), which together with the phylogenetic data suggests that *erg6b* and *erg6c* may not be as biologically relevant during standard growth conditions. Therefore, we named the *Mucor* paralogs Erg6a, Erg6b, and Erg6c in agreement with our evolutionary model (Figure 2E), phylogenetic, and transcriptomic data, and we reasoned that *erg6a* deletion may suffice to confer loss of Erg6 function.

To explore the role of the *erg3* and *erg6a* genes in mucoralean ergosterol biosynthesis, antifungal susceptibility, and pathogenesis, we generated deletion mutant strains in *M. circinelloides* and *M. lusitanicus* (Figure S5). The genetic loci were successfully replaced through homologous recombination by uracil prototrophy markers: *pyrF* for *M. circinelloides* (Figure S5A-B), utilizing the newly designed MIN6 strain and genetic transformation via electroporation procedure; and *pyrG* for *M. lusitanicus* (Figure S5C-D), using a previously described transformation method (48). Be-

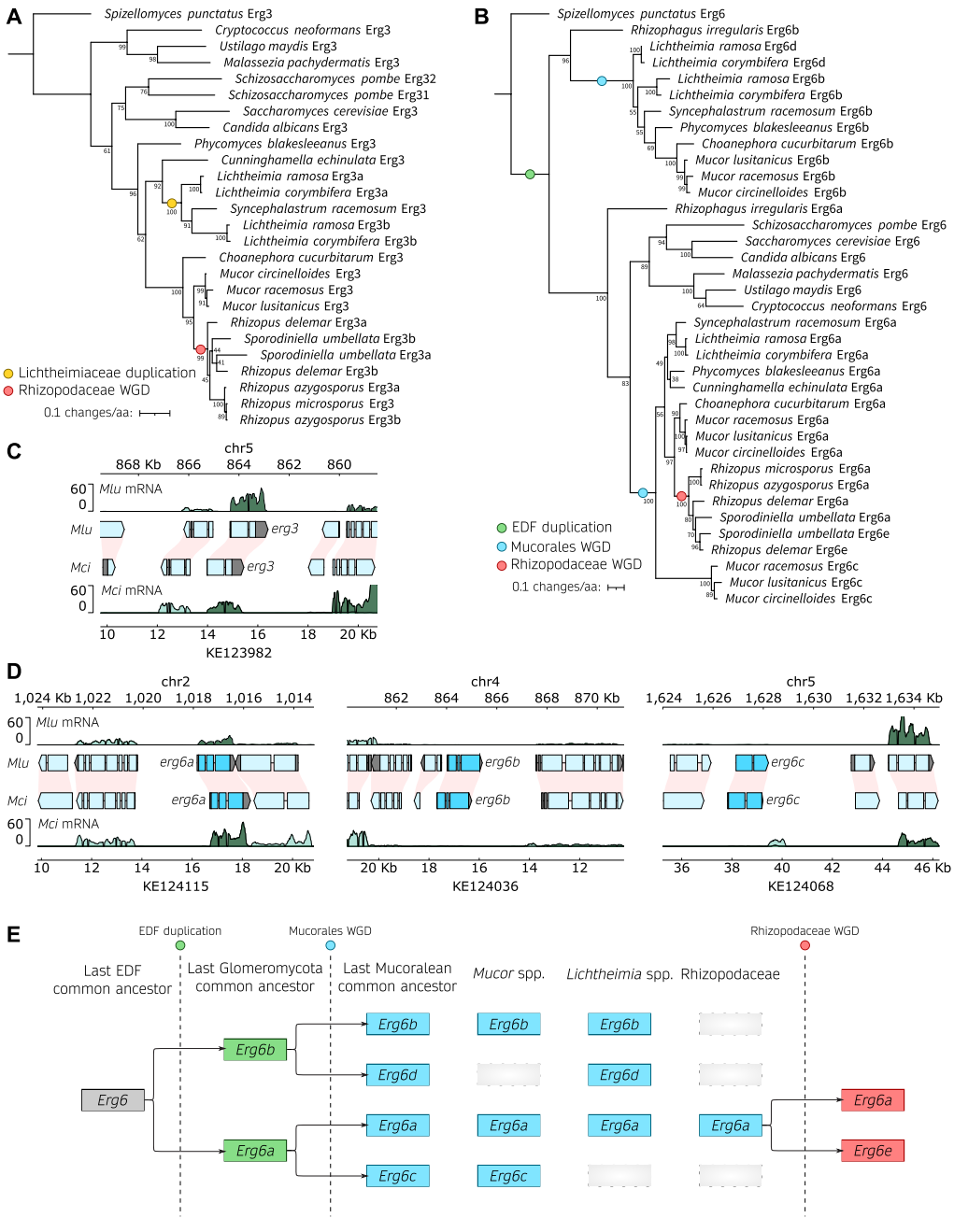

Figure 2. Erg3 and Erg6 evolutionary history across the Mucoromycota. (A, B). Phylogenetic tree depicting the Erg3 **(A)** and Erg6 **(B)** amino acid sequence alignments in clinically relevant fungi, with a specific focus on Mucorales. The Erg protein sequences from the chytrid *Spizellomyces punctatus* were employed as outgroups to root the trees. Additionally, the Erg6 sequence from *Rhizophagus irregularis*, a member of the Glomeromycota and the closest non-Mucoromycota sequence, was included to provide clarity on duplication events in **(B)**. Noteworthy branching events, including whole genome duplications (WGD) or gene duplications, are denoted by color-coded circles. Node support is represented as a percentage based on 1,000 bootstrapping iterations. The branch length is scaled to 0.1 substitutions per amino acid, as indicated in the legend. **(C, D).** Plots illustrating gene transcription across *M. lusitanicus* (*Mlu*) and *M. circinelloides* (*Mci*) genomic regions containing *erg3* **(C)** and *erg6* orthologs **(D)**. The genomic coordinates for both species are displayed above (*Mlu*) and below (*Mci*) each plot. Gene annotation is depicted as arrowed blocks, indicating the direction of transcription and the boundaries of exons and introns. The coloring scheme assigns cyan blue to *erg* coding sequences, light blue to the remaining coding sequences, and gray to untranslated regions. Interspecies synteny among genes is depicted as pink shading. Gene transcription is shown as rRNA-depleted RNA read coverage, with the forward strand represented in dark green and the reverse strand in light green, enabling assessment of sense and antisense transcription. In some instances, the x-axes were inverted, and in those cases, the forward and reverse strand orientations were also inverted to enhance visualization and clarification. **(E)** Model illustrating the inferred evolutionary history of Erg6 across the early-diverging fungi (EDF).

cause Mucorales have non-septate hyphae and multinucleated spores, transformed protoplasts frequently harbor wild-type and mutant nuclei simultaneously, a phenomenon known as heterokaryosis. To lose the wildtype nuclei and obtain exclusively homokaryotic deletion mutants, transformants must be cultured for several asexual generations in a medium that positively selects the mutant nuclei. After this process of mutant nuclei enrichment, *erg3*Δ and *erg6a*Δ homokaryotic mutations were verified by PCR-amplified fragment length polymorphism (AFLP, Figure S5), and two independently generated homokaryotic mutants were selected for each deletion to ensure phenotypic specificity in subsequent studies.

***erg3* and *erg6a* deletion affects growth and virulence in *M. circinelloides*.** Alterations in ergosterol composition may affect the stability of biological membranes and usually lead to fitness impairments. Consequently, we examined the effects of loss-of-function mutations in the *erg3* and *erg6a* genes of *M. circinelloides* and *M. lusitanicus*, specifically focusing on evaluating defects in various aspects of fitness, including growth rate, sporulation, and virulence. For these and subsequent analyses, data from each pair of independently generated mutants harboring the same gene deletion were grouped for simplicity when necessary for primary figures, after ensuring that there were not significant differences between them as can be observed in the supplementary information (Figures S6-S8, and Data set S1). The growth rate was evaluated at different temperatures, including optimal growth and human physiological temperatures

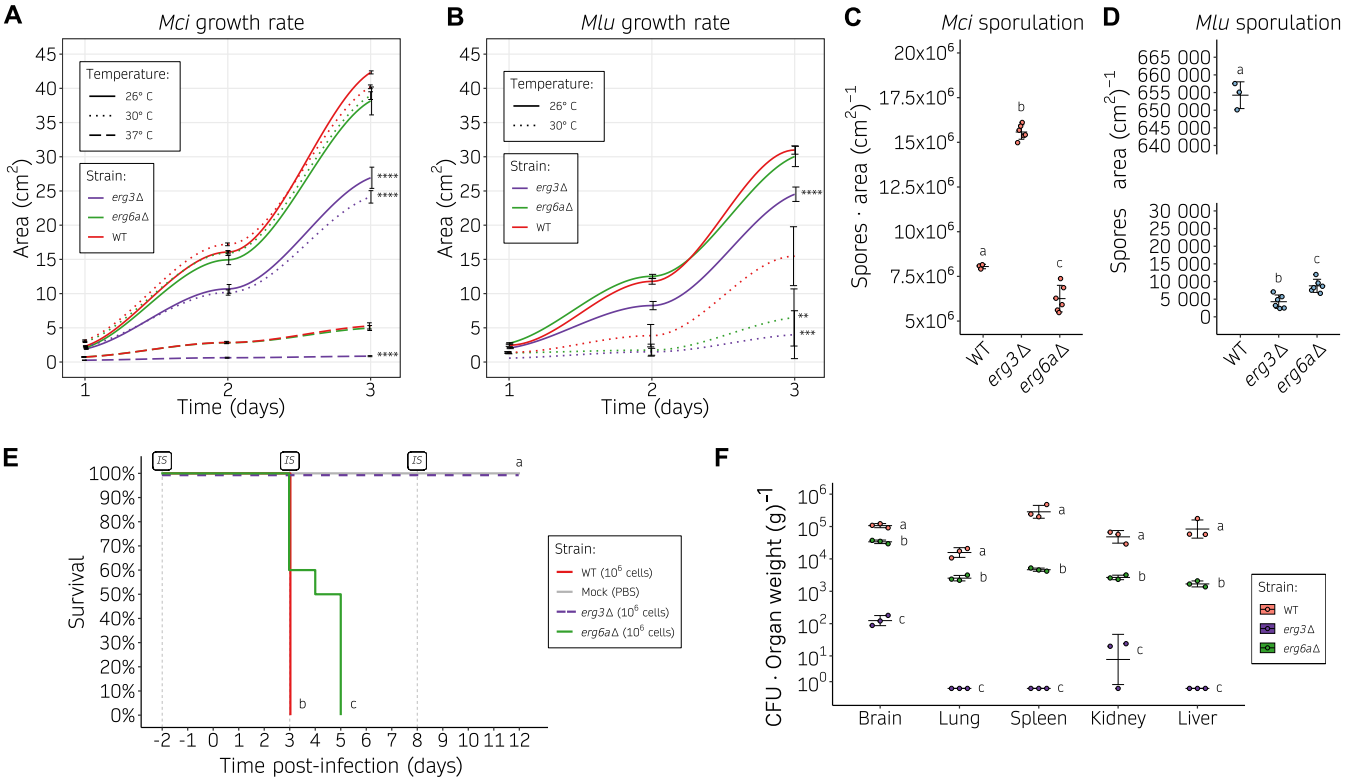

Figure 3. Alterations in the ergosterol biosynthetic pathway result in decreased growth rate, sporulation, and virulence. (A, B) Growth rate of *M. circinelloides* **(A)** and *M. lusitanicus* **(B)** *erg3*Δ and *erg6a*Δ (shown as color-coded lines) in rich medium at different temperatures (shown as distinct line types), measured as colony area across 24-hour intervals. Individual values were determined either in six biological replicates for the wild type or in three biological replicates of two independently generated mutants (six total values, grouped together for simplicity as no significant differences were detected), and used to plot a smoothed curve and SD values as black lines. Significant area differences in depicted strains compared to the wildtype growth rate across the whole time-course were determined by a One-way ANOVA and Tukey HSD test for each temperature group and shown as asterisks (** *p-value* $\leq$ 0.01, *** *p-value* $\leq$ 0.001, and **** *p-value* $\leq$ 0.0001). **(C, D)**. Sporulation rate of *M. circinelloides* **(C)** and *M. lusitanicus* **(D)** *erg3*Δ and *erg6a*Δ after a 72-hour incubation at room temperature in rich medium, determined as number of spores per cm^2. Values from individual measurements were obtained from three biological replicates of either the wildtype strain or two independently generated mutants (grouped together as no significant differences were found). These values are depicted in a dot plot, with standard deviation (SD) values represented as black lines. Strains are grouped by letters showing significant sporulation differences determined by a One-way ANOVA and Tukey HSD test (*p-value* $\leq$ 0.01). **(E)** Kaplan-Meier survival curves of immunosuppressed mice after infection with *M. circinelloides* wildtype and ergosterol mutants (color-coded). For *erg3*Δ and *erg6a*Δ, two independently generated mutants were injected into groups of 5 mice. For simplicity, after observing no significant differences in the results, the mice were grouped together per gene deletion in groups of 10. Intraperitoneal immunosuppressive (IS) treatments are shown. Strains showing significant differences in virulence are indicated as different letters (*p-value* $\leq$ 0.01), assessed by a Log-rank test. **(F)** Fungal burden at 3 days post-infection in immunosuppressed mice, measured as colony-forming units (CFU) per gram of five different organs. SD and mean (black lines) were assessed from 3 biological triplicates. For each organ category, strains are grouped by letters showing significant fungal burden differences (One-way ANOVA and Tukey HSD test, *p-value* $\leq$ 0.01).

(Figure 3A-B). The *M. circinelloides erg3*Δ mutant exhibited a significant growth delay under all conditions tested (26 °C, 30 °C, and 37 °C) compared to the wild type, whereas the *M. circinelloides erg6a*Δ mutation did not affect growth significantly (Figure 3A). The same growth trends were observed in minimal media (Figure S6A). Similarly, the *M. lusitanicus erg3* mutant displayed growth defects under every condition (26 °C and 30 °C), while the *erg6a* mutant showed a growth delay only at 30 °C (Figure 3B). As *M. lusitanicus* is not able to withstand human physiological temperatures (37 °C), and exhibits a considerably lower optimal growth temperature (26 °C), this could explain the interspecies differences observed. Notably, increasing the temperature range beyond the optimal growth temperature for each species (37 °C for *M. circinelloides* and 30 °C for *M. lusitanicus*) severely affected the growth rate in every strain, including the wildtype controls but more importantly, rendered the phenotype confirmed by *erg* gene deletions more severe.

Asexual sporulation was also affected by *erg* mutations in *M. circinelloides* and *M. lusitanicus*. In *M. circinelloides*, the *erg3*Δ mutant displayed a significant increase in sporulation, as opposed to the decrease observed in the *erg6a*Δ mutant compared to the wildtype strain (Figure 3C). Interestingly, *M. circinelloides erg3*Δ mutants exhibit a higher number of sporangiophores packed more closely together towards the center of the colony, which may explain their increase in sporulation rate. On the other hand, the differences observed in *M. lusitanicus* were more severe compared to their wildtype strain. Both *erg3*Δ and *erg6a*Δ mutants showed a substantial and significant reduction in sporulation (Figure 3D), characterized by a paucity of sporangiophore production.

The observed differences in both growth and sporulation imply that deletion of the *erg3* and *erg6a* genes could impact fitness under various stress conditions, particularly temperature. To investigate whether these defects are relevant during the infection process, a survival assay was conducted using *M. circinelloides* strains, as they are able to withstand murine physiological temperatures and exhibit a more reli-

able pathogenic potential. Immunosuppressed mice were infected with two independently generated mutants for each gene, and with the wildtype strain 1006PhL (Figure 3E and Figure S7). Mice meeting endpoint criteria were sacrificed and fungal burden was determined, ensuring mice infected with every independently generated mutant were utilized. Although *erg6a*Δ mutants exhibited attenuated virulence compared to the wildtype control, they were able to establish a fully disseminated infection resulting in mortality among all infected mice. Conversely, all of the mice infected with *erg3* mutants survived, possibly due to a significant and drastic reduction in fungal burden within vital organs (Figure 3E-F). These findings suggest that *erg3* deletion abolishes virulence in *M. circinelloides*, whereas *erg6a* deletion may not suffice to prevent dissemination and mortality.

Taken together, these results confirm that deletion of *erg3* and *erg6a* leads to a reduction in fitness in specific settings and particularly at higher than optimal temperatures, observing a higher fitness cost for *M. lusitanicus*, and confirming interspecies differences between *M. circinelloides* and *M. lusitanicus*. As expected, this *erg* deletion-related loss of fitness impacts the virulence potential of *M. circinelloides*, more profoundly as a consequence of *erg3* deletion, and slightly due to *erg6a* deletion. Although *erg6a* deletion leads to delayed infection, it is noteworthy that this strain is still able to cause full mortality.

Table 1. Amphotericin B (AMB), posaconazole (POS) and isavuconazole (ISA) minimal inhibitory concentration (MIC) for *M. circinelloides* and *M. lusitanicus erg3*Δ and *erg6a*Δ mutants.

Strain	AMB (mg/L)	POS (mg/L)	ISA (mg/L)
M. circinelloides			
WT 1006PhL	0.125	2	8
*erg3*Δ-1	0.25	0.5	4
*erg3*Δ-2	0.25	0.5	4
*erg6a*Δ-1	0.5	1	8
*erg6a*Δ-2	0.5	1	8
M. lusitanicus			
WT MU636	0.03125	0.5	4
*erg3*Δ-1	0.125	0.125	2
*erg3*Δ-2	0.125	0.125	2
*erg6a*Δ-1	0.5	0.25	2
*erg6a*Δ-2	0.5	0.25	2

***erg6a* loss-of-function mutations result in antifungal drug resistance.** The antifungal drug susceptibility profiles of *erg3*Δ and *erg6a*Δ mutants were conducted following the CLSI and EUCAST standard methodology for filamentous fungi, determining the minimal inhibitory concentration values required to inhibit growth (MIC) by broth microdilution (Table 1). As there are only three clinical antifungal drugs recommended for mucormycosis treatment –the liposomal formulation of amphotericin B (Ambisome), posaconazole (Noxafil), and isavuconazonium sulfate (Cresemba)– susceptibility testing was focused on those drugs. Both *M. circinelloides* and *M. lusitanicus* exhibited similar trends in MIC values, indicating generalizable alterations in antifungal drug susceptibilities. First, *erg3* deletion profoundly affected antifungal susceptibility. A minor increase in MIC was observed for amphotericin B, with a 2-fold and 4-fold increase observed in *M. circinelloides* and *M. lusitanicus*, respectively. Conversely, *erg3*Δ mutants also exhibited a significantly increased susceptibility to azoles, as evidenced by a 4-fold decrease in MIC for posaconazole, and a 2-fold decrease for isavuconazole in both *M. circinelloides* and *M. lusitanicus*. Second, the e*rg6a*Δ mutants showed substantial resistance to amphotericin B, specifically a 4-fold and 16-fold MIC increase in *M. circinelloides* and *M. lusitanicus*, respectively. These *erg6a*Δ mutants also exhibited a slightly increased susceptibility to azoles, manifested by a 2-fold MIC decrease for posaconazole and isavuconazole in *M. lusitanicus*, and a 2-fold decrease for posaconazole in *M. circinelloides*.

Antifungal drug susceptibility testing in molds by broth microdilution is challenging and subject to qualitative interpretation. More importantly, it is difficult to account for the inherent growth defects that are present in *erg3* and *erg6a* deletion strains. An alternative method was employed to address this issue, measuring antifungal drug susceptibility as the area of inhibited growth on solid media, normalizing to growth without drug. To obtain a dynamic quantification of drug susceptibility, area measurements were taken at different time points (Figure 4 and Figure S8). The differences in drug susceptibility became more evident on day 2 (Figure 4A), as indicated by a plateau in the growth inhibition curves between days 2 and 3 (Figure 4B-C). Growth inhibition was stronger on day 1 in every condition tested and stabilized after day 2, suggesting that polyenes and azoles also restrict germination in addition to growth. The *erg3*Δ mutants of *M. circinelloides* and *M. lusitanicus* showed increased susceptibility to both azoles –posaconazole and isavuconazole– and this hypersusceptibility was more severe under isavuconazole stress. Similarly, amphotericin B resistance was confirmed in *erg6a*Δ mutants for both *Mucor* species, and in *M. circinelloides erg3*Δ mutants. *M. lusitanicus erg6a*Δ mutants also showed increased sensitivity to azole drugs, overall confirming that these differences in susceptibility observed in the MIC tests (Table 1) were significant and independent of their inherent growth defects. Taken together, our results indicate that *erg3* deletion results in azole hypersusceptibility, whereas *erg6a* deletion confers polyene resistance in *Mucor* species. These differences in the mutants indicate that modifying the ergosterol biosynthetic pathway, and consequently, the content of ergosterol and intermediate sterols, may contribute to the mucoralean drug susceptibility changes that we aim to address further.

Ergosterol profile alteration as the underlying mechanism of antifungal drug resistance. The C-5 desaturase Erg3 and C-24 methyltransferase Erg6 are indispensable components of the ergosterol biosynthetic pathway, responsible for converting lanosterol into ergosterol through a series of catalytic reactions performed by these and other Erg enzymes. Loss-of-function of either enzyme has been shown to alter the ergosterol and related sterol composition

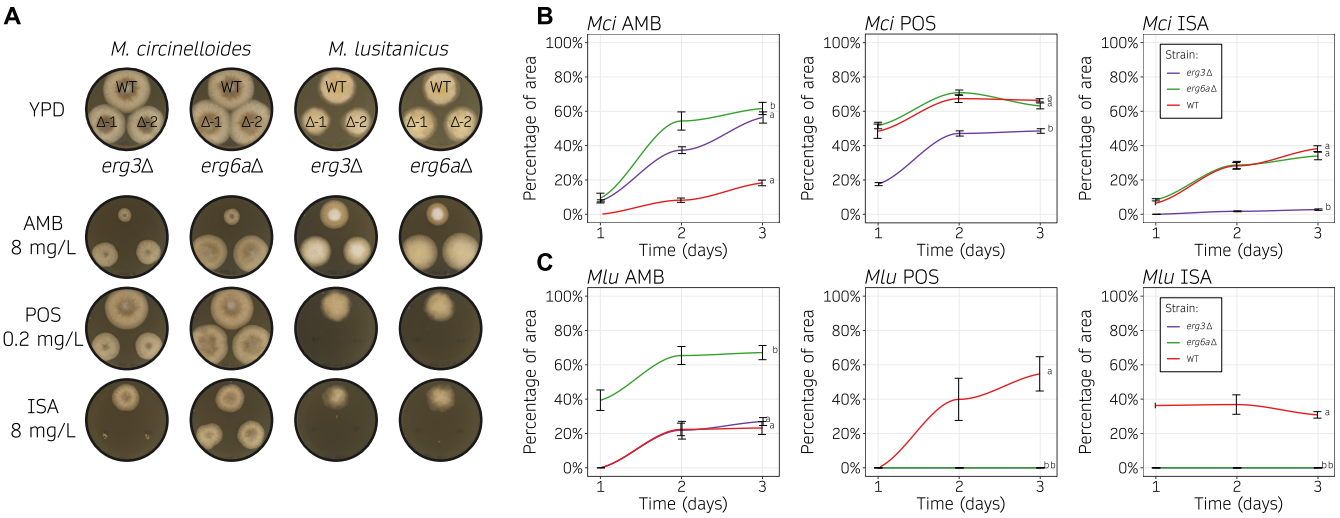

Figure 4. Loss of Erg3 or Erg6a function leads to changes in azole and polyene susceptibility. (A, B, C) Amphotericin B (AMB, 8 mg/L), posaconazole (POS, 0.2 mg/mL), and isavuconazole (ISA, 8 mg/mL) susceptibility testing of wild type and ergosterol mutants using solid media. Each species was assayed at its optimal temperature, 30 °C and 26 °C for *M. circinelloides* (*Mci*) and *M. lusitanicus* (*Mlu*), respectively. In **(A),** representative images of growth after 48 hours in all the depicted media, including the control medium without drug (YPD). Two independently generated mutants were assayed for each gene deletion (Δ-1 and Δ-2). In **(B, C)**, *Mci* **(B)** and *Mlu* **(C)** growth rates from each mutant across time (24-hour intervals) were determined as the percentage of growth area from the same strain cultured in control medium without drug. Individual values were determined either in six biological replicates for the wild type or in three biological replicates from two independently generated mutants (six total values, grouped together for simplicity as no significant differences were detected), and used to plot a smoothed curve and SD values as black lines. Strains were grouped by letters showing significant growth rate differences across the whole time-course (One-way ANOVA and Tukey HSD test, *p-value* $\leq$ 0.01).

in other organisms (43, 44), and we hypothesized that deletion of the *erg3* or *erg6a* genes in *Mucor* species might similarly modify their sterol profiles, explaining the observed changes in antifungal drug susceptibility. To test this hypothesis, we analyzed the sterol profiles of *M. circinelloides* wildtype, *erg3*Δ, and *erg6a*Δ strains by gas chromatography and mass spectrometry (Figure 5 and Data set S1). Sterols were classified into different categories: C-5(6)-desaturated ergosta-type sterols, C-5(6)-saturated ergosta-type sterols, C-14-methylated sterols, and cholesta-type sterols. This classification aims to simplify sterol characterization and emphasize the accumulation of sterols that may result from Erg3 or Erg6 loss-of-function, as well as exposure to polyene or azole treatments. It is important to note that several sterols classified as cholesta-type may also exhibit C-5(6) desaturation or C-14 methylation.

First, we focused on the sterol profile of *M. circinelloides* cultured in rich medium, beginning with the wildtype strain and then the *erg3*Δ and *erg6a*Δ mutants. The relative ergosterol content was lower in *M. circinelloides* wild type (34.3 ± 7.2 %) than in other fungi (23, 26, 49, 50), yet it remains the most abundant sterol (Figure 5A and Data set S1). Intriguingly, we found relatively high levels of C-5(6)-saturated sterols [fecosterol (6.0 ± 0.7 %), episterol (4.5 ± 1.7 %), ergosta-7,22,24(28)-trienol (11.7 ± 3.6 %), and others (7.9 ± 2.4 %)], as well as C-14-methylated sterols [lanosterol (4.0 ± 2.0 %), eburicol (12.2 ± 2.9 %), and others (3.5 ± 2.8 %)]. These results indicate that other ergosta-type sterols may act as essential components of *M. circinelloides* membranes in addition to ergosterol. *M. circinelloides erg3* deletion resulted in a considerable increase in C-5(6)-saturated sterols [episterol (26.9 ± 4.2 %) and others (26.3 ± 3.6 %)]; notably, these include elevated levels of ergosta-7,22-dienol (37.0 ± 6.7 %), which was not detected in the wild-type strain. More importantly, *erg3*Δ mutation led to complete depletion of C-5(6)-desaturated ergosta-type sterols, including ergosterol, confirming a complete loss of Erg3 function. On the other hand, *erg6a* deletion caused a decrease in ergosterol (28.9 ± 5.2 %) and an increase in C-24-non-methylated sterols [lanosterol (29.8 ± 7.7 %) and cholesta-type sterols (13.9 ± 2.5 %)], confirming Erg6a activity as a C-24 methyltransferase and suggesting a partial loss of Erg6 function. As *M. circinelloides erg6a*Δ mutants are still capable of producing C-24-methylated sterols, including ergosterol, it indicates that in the absence of Erg6a activity, additional Erg6 copies –Erg6b and Erg6c– might be upregulated and function as C-24 methyltransferases to partially rescue *erg6a* deletion, though not completely. These findings are consistent with Erg6a serving as the primary Erg6 enzyme, as Erg6a loss-of-function significantly redirects the ergosterol biosynthetic pathway towards the production of cholesta-type sterols, which is indicative of a severe Erg6 deficiency (Figure 5B, Figure S9, and Figure S10A). The relative abundance of eburicol and absence of zymosterol in the wildtype strain, together with higher relative amounts of lanosterol compared to zymosterol in *erg6a*Δ mutants, evidence that Erg6 precedes Erg11 activity on lanosterol, delimiting the preferred ergosterol biosynthetic pathway in *M. circinelloides* (Figure 5B and Figure S9, center lane).

Next, we analyzed the sterol profile of the wildtype and mutant strains after amphotericin B treatment. Polyene, such as amphotericin B, binding to ergosterol leads to fungal cell death, and is usually correlated with a drastic decrease in ergosterol (10, 11). Indeed, the normalized amount of ergosterol was considerably lower in every strain treated with amphotericin B (Figure S11). The relative sterol contents of

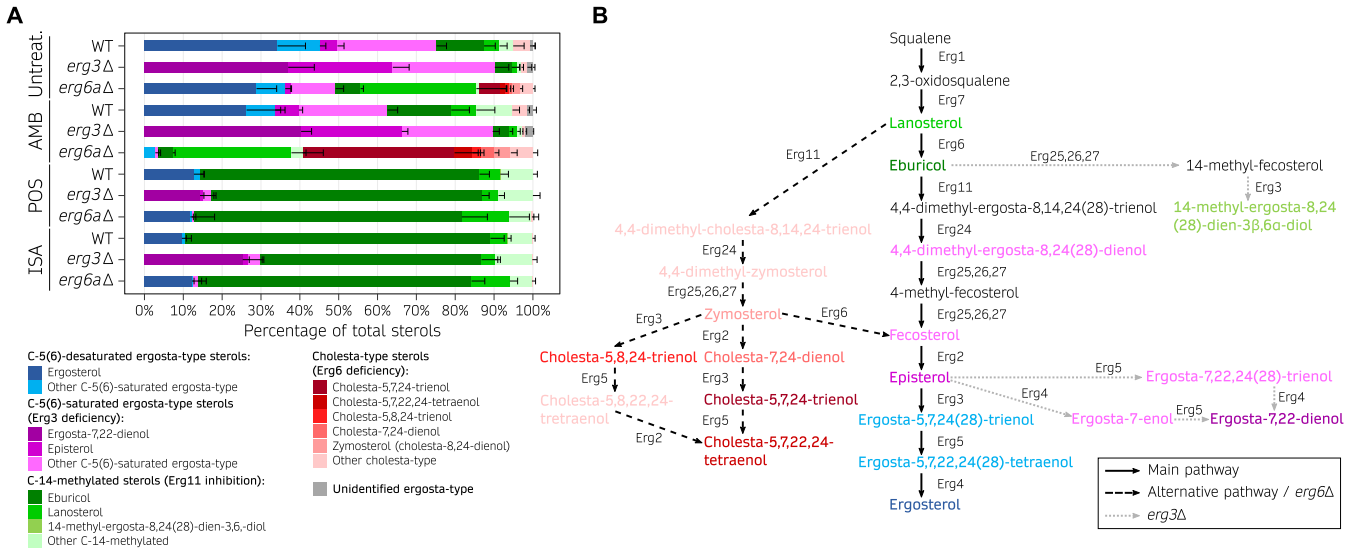

Figure 5. Ergosterol composition upon exposure to first-line mucormycosis treatments is altered by Erg3 and Erg6a deficiencies. (A) Percentage of total sterols in *M. circinelloides* wildtype (WT), *erg3*Δ, and *erg6a*Δ strains when exposed to different antifungal treatments (amphotericin B, posaconazole, and isavuconazole) and untreated cultures, represented in a stacked bar plot. Mean and SD (only upper bound is shown) values were determined from 6 replicates in the WT strain; for each mutation and condition, two independently generated mutants were tested in triplicate (total of 6 replicates). Sterols are classified in four main categories that reflect the expected end products from the main ergosterol pathway (C-5(6)-desaturated sterols), Erg3 deficiency (C-5(6)-saturated sterols), Erg6 deficiency (cholesta-type sterols), and Erg11 inhibition due to azole exposure (14-methylated sterols). Within each category, the most abundant sterols are color-coded to facilitate visualization. **(B)** Model of the ergosterol biosynthetic pathway in Mucorales. The main pathway is depicted by straight, black arrows. Alternative pathways that are relevant in *erg3* (dashed, black arrows) or *erg6a* deletions (dotted, gray arrows) are also shown. For better illustration, sterol compounds are classified and color-coded as in **(A)**.

amphotericin B-treated *M. circinelloides* wildtype and *erg3*Δ mutant strains were similar to their untreated cultures, except for a marked decrease in ergosterol in the wild type (26.3 ± 9.9 %). On the other hand, the relative sterol profile of the *erg6a*Δ mutant was substantially altered by polyene treatment, resulting in a total absence of ergosterol production, abolishment of most C-5(6)-saturated sterols except for fecosterol, which exhibited a drastic decrease (0.8 ± 0.6 %), and more importantly, a near 60 % relative abundance of cholesta-type sterols [cholesta-5,7,24-trienol (39.1 ± 6.7 %) and others (20.2 ± 2.4 %)] (Figure 5A and Data set S1). *M. circinelloides erg6a*Δ mutants exhibit increased resistance to amphotericin B, suggesting that cholesta-type sterol-based membranes are sufficiently stable and that producing these sterols as an alternative to ergosterol may protect the fungus against polyene treatment.

Finally, the sterol content in these strains was also assessed after exposure to two different azoles: posaconazole and isavuconazole. These drugs are the only azoles recommended for salvage therapy against mucormycosis. Azoles target the Erg11 enzyme, inhibiting the crucial C-14 sterol demethylase activity responsible for converting lanosterol or eburicol into the subsequent C-14-demethylated sterol intermediate, ultimately leading to ergosterol (Figure 5B, Figure S9, and Figure S10B). In many fungal species, this blockade in the ergosterol biosynthetic pathways redirects the sterol flow into a different pathway that leads to the accumulation of the toxic sterol 14-methyl-ergosta-8,24(28)-dien-3,6-diol, which is the cause of the azole antifungal effect. Indeed, the sterol profile revealed that exposure to either azole drug led to the overaccumulation of C-14-methylated sterols, mainly eburicol (71.9 ± 2.5 % in cells treated with posaconazole and 78.7 ± 3.5 % with isavuconazole); and a substantial decrease in ergosterol (12.7 ± 2.6 or 9.6 ± 2.4 % with posaconazole or isavuconazole, respectively) and other ergosta-type sterols (Figure 5A and Data set S1). But surprisingly, azole treatment did not result in an overaccumulation of the toxic 3,6-diol or its precursor 14-methyl-fecosterol, both frequently found in large proportions in other fungal species (12). Only trace amounts of the toxic 3,6-diol (0.2 ± 0.1 %) were found in the wildtype strain during exposure to both azoles, while *erg3*Δ mutants did not produce the toxic 3,6-diol at all (Figure 5A and Data set S1). These findings reveal that although *M. circinelloides* Erg3 is capable of catalyzing this step, there is a limited utilization of the pathway responsible for converting eburicol into toxic sterols during azole exposure (Figure S10B-C), and are particularly intriguing given the susceptibility of *M. circinelloides* to posaconazole and isavuconazole. Notably, the hypersensitivity of the *erg3*Δ mutants to these azoles implies that the antifungal effect results from the absence of ergosterol and other stable sterols in the cellular membranes (Figure 5A and Data set S1).

Taken together, our findings define the preferred ergosterol biosynthetic pathway in *M. circinelloides* (Figure 5B and Figure S9, center lane) and reveal that Erg3 and Erg6a play critical roles in antifungal drug susceptibility. The *erg6a* deletion neither impairs growth nor abolishes virulence completely, but results in a decreased Erg6 activity and therefore, an abundance of stable cholesta-type sterols over ergosterol during exposure to amphotericin B that accounts for the antifungal resistance observed in *erg6a*Δ mutants. In addition, despite *erg3*Δ leading to increased susceptibility to azoles, we could not detect an abundance of toxic 14-methyl-ergosta-8,24(28)-dien-3,6-diol during azole exposure, suggesting that

lacking critical sterols for proper membrane function is driving posaconazole and isavuconazole antifungal effect in Mucorales.

Discussion

Mucormycoses are fungal infections that present with various clinical manifestations, respond differently to therapy, and result in varying outcomes. These infections are as diverse as the distinct species responsible for causing the disease. Indeed, mucoralean fungi display interspecies differences in antifungal drug susceptibility (2, 51) and interactions with host immunity (52), which can explain disease heterogeneity, and these considerations emphasize the importance of specific pathogenicity models in mucormycosis research. However, these species remain understudied and there are only a limited number of genetic models available to study host-pathogen interactions, dissemination mechanisms, and therapeutics. Recent taxonomic advances revealed that many strains and clinical isolates previously classified as *M. circinelloides* actually belong to different phylogenetic species within the *M. circinelloides* species complex (29). Among these, *M. circinelloides* is the most frequently isolated species from mucormycosis patients. However, all of the studies investigating the molecular mechanisms of pathogenicity have been conducted with *M. lusitanicus*, a sister species previously classified as *M. circinelloides* f. *lusitanicus*, for which no clinical isolates have been found to date (29). This work aims to address these limitations by developing a new molecular biology model based on a pathogenic human isolate of *M. circinelloides*, known as strain 1006PhL. As a result of this study, this strain is now amenable to genetic transformation and exhibits full virulence in the immunosuppressed murine model. Mortality rates in animals infected by this strain are consistently high and reproducible, as well as fungal burden quantification assays, partially due to the ability of this pathogenic isolate to grow within the range of mammalian physiological temperatures. This thermotolerance offers additional advantages, allowing for antifungal drug susceptibility testing following standard procedures specified by CLSI and EUCAST for filamentous fungi, which need to be conducted at 35 °C. Our research has demonstrated that deletion of key target genes, such as *pyrF*, results in a completely avirulent phenotype, which can be reversed by genetic complementation via genomic integration. The necessity of PyrF and the pyrimidine biosynthetic pathway for virulence is in agreement with research in other fungal model organisms (41, 53–55), demonstrating that this model is suitable for virulence factor characterization and establishing a foundation for novel molecular pathogenesis research to follow.

The only available antifungal agents effective against mucormycosis, namely azoles and polyenes, modify the ergosterol content, emphasizing the crucial role of ergosterol biosynthesis in antifungal drug susceptibility. For instance, gain-of-function mutations affecting Erg11, the target of azole drugs, typically confer azole drug resistance in many fungal pathogens (56). Similarly, Mucorales exhibit intrinsic resistance to voriconazole and fluconazole due to an Erg11 duplication with an amino acid substitution affecting the azole binding site (6). Mucorales can develop antifungal drug resistance not only through classical genetic point mutations (6) and insertional mutations (57), but also via epigenetic modifications that lead to transient loss of drug target function (8, 57, 58). Therefore, this study focuses on characterizing loss-of-function mutations affecting ergosterol biosynthetic enzymes Erg3 and Erg6, and their effect on growth, virulence, and most importantly, antifungal drug resistance and sterol content in two different *Mucor* species: *M. circinelloides* and *M. lusitanicus*. Our findings elucidate the preferred ergosterol biosynthetic pathway in *M. circinelloides*, indicating that C-24 methylation catalyzed by Erg6a occurs prior to C-14 demethylation by Erg11. This result is consistent with our understanding of ergosterol biosynthesis in other filamentous fungi (50), as well as in *Candida* species (16, 23, 43) and *Cryptococcus neoformans* (59), which deviates from the ergosterol pathway proposed in *Saccharomyces cerevisiae* (60). However, the relative content of ergosterol in *M. circinelloides* is reduced compared to these other fungal species, while other sterols such as episterol, lanosterol, and eburicol are more abundant. There is a common misconception that ergosterol is the sole sterol found in all fungi and is essential for fungal membrane stability. While it may be the dominant sterol in many of the Dikarya fungi, there is substantial evidence of alternative sterols serving the same role in other fungi, especially early-diverging fungi (EDF) (61). Most EDF lack Erg5 and even Erg11, and instead harbor a different set of sterol biosynthetic enzymes, such as 7-dehydrocholesterol reductase (DHCR7), resulting in a wider diversity of sterols and a complete absence of ergosterol (61, 62). While this is not the case in most Mucoromycota species, our research reveals that they possess at least two Erg6 paralogs, and *Mucor* species harbor three: Erg6a, Erg6b, and Erg6c. These additional Erg6 paralogs, which are putative C-24 methyltransferases, may be responsible for *M. circinelloides* unique sterol composition, particularly the abundance of C-24-methylated sterols. As a sister clade to the Dikarya, Mucoromycota represents their closest EDF relatives and therefore, displays a hybrid sterol composition profile between more phylogenetically distant EDF and well-studied Dikarya. Taken together, our findings provide new insights into the evolution of membrane sterol composition in fungi, showing evidence of alternative sterol pathways.

Dissecting the role of the C-5 sterol desaturase Erg3 in the ergosterol pathway of *M. circinelloides* uncovered unexpected peculiarities. The sterol profile of *erg3*Δ mutants showed a total absence of ergosterol, regarded as the essential sterol of fungal membranes. Nevertheless, our findings indicate that *Mucor* species are able to survive on alternative sterol intermediates, as has been previously reported in *C. glabrata erg11* mutants (63), and similarly to EDF species naturally lacking ergosterol (61, 62). The altered sterol composition may explain the growth delay observed in *erg3*Δ mutants at optimal temperatures, which becomes more pronounced at higher temperatures, as well as the mutants' com-

plete loss of virulence. Reasonably, the changes in sterol content, possibly accompanied by compensating alterations in other membrane lipids, can cause an unstable equilibrium that enables growth in non-stressful conditions but collapses upon harsh environmental changes, particularly during thermal stress and host interactions. These findings align with the observed *erg3* loss-of-function mutations in *Candida* species, which exhibit increased susceptibility to physiological stresses (64, 65) and reduced hyphal growth under certain conditions (66). Consequently, many of these *erg3* null mutants of *Candida* species have been associated with reduced pathogenicity in animal models, albeit these azole resistant, *erg3* mutant isolates originated from human patients (19, 65, 66), and some compensatory mutations can restore their pathogenic potential (17). In addition to these defects, *erg3* loss-of-function mutations confer azole resistance in nearly every *Candida* species (13, 16–20, 64, 65, 67), which might be the reason they are so frequently identified from clinical isolates. Azoles block ergosterol synthesis by inhibiting the C-14 sterol demethylase Erg11, causing an accumulation of Erg11 substrates: lanosterol and eburicol. Typically, these substrates are redirected to a different pathway characterized by the production of 14-methyl-fecosterol through the subsequent action of Erg25, Erg26, and Erg27, which is turned into the toxic 14-methyl-ergosta-8,24(28)-dien-3,6-diol through Erg3 C-6 hydroxylase activity. Lacking Erg3 activity prevents the formation of the toxic diol while accumulating 14-methyl-fecosterol, accounting for the observed resistance in the *Candida erg3* null mutants (43, 68). Because the loss of Erg3 function halts ergosterol synthesis completely in *Candida* species, polyenes are not able to bind the cell membrane and exert their antifungal effects. As a result, these mutants often exhibit resistance not only to azoles but also to polyenes such as amphotericin B (15, 16, 69, 70). *M. circinelloides erg3*Δ mutants are also more resistant to amphotericin B and, as in *Candida* species, this is likely due to a complete absence of ergosterol that prevents polyene binding. However, these mutants are hypersensitive to azole drugs instead of more resistant, and neither the wildtype nor the mutant strains produce the toxic 14-methyl-3,6-diol. This finding suggests that Erg3 may exhibit a limited capability for C-6 hydroxylation of C-14-methylated sterols compared to other fungi. Nevertheless, the overaccumulation of eburicol in *M. circinelloides erg3*Δ mutants during azole exposure, together with absence of 14-methyl-fecosterol and 4,14-dimethyl-cholesta-8,24-dienol, imply that the Erg25, Erg26, and Erg27 enzymes may prefer different substrates other than eburicol or are simply unable to initiate C-4 demethylation on 14-methylated sterols as more likely scenarios. This sterol composition with abundant eburicol and absence of 14-methyl-fecosterol or ergosterol could hinder growth and cell membrane function, explaining the hypersensitivity to azoles in *M. circinelloides erg3*Δ mutants and the differences compared to *Candida* species.

This study further investigates Erg6, a C-24 methyltransferase that catalyzes an essential step in the biosynthesis of ergosterol. Erg6 function has been studied in several fungal pathogens and revealed as important for growth and development under various conditions, adaptation to cell wall stresses, virulence (23–27), and in some instances, essential for cell viability (50). Despite these defects, the absence of Erg6 activity can provide a selective advantage by conferring polyene drug resistance, as seen in multiple *Candida* species and *Cryptococcus neoformans* (22–27). Exploring the function of Erg6 in *Mucor* species presented additional challenges due to the presence of three different Erg6 paralogs. Our phylogenetic and transcriptomic analyses identified Erg6a as the primary Erg6 enzyme involved in *Mucor* species ergosterol biosynthesis. This hypothesis was confirmed by a substantial reduction in C-24-methylated sterols in the *erg6a*Δ mutants, although some residual Erg6 activity persisted. Therefore, Erg6b and/or Erg6c might serve as functionally redundant C-24 methyltransferases in the absence of Erg6a, accounting for the residual Erg6 activity. As in other fungal species, *Mucor* species *erg6a*Δ mutants exhibit defects in asexual sporulation, a significant delay in virulence, and decreased host dissemination. More importantly, *erg6a*Δ mutants are highly resistant to amphotericin B. The sterol profile of *erg6a*Δ mutants under amphotericin B exposure provided insights into the mechanism of polyene resistance. It revealed an abundance of cholesta-type sterols, which bear a closer resemblance to cholesterol found in animal cell membranes. A similar sterol profile was observed in amphotericin B-resistant *C. auris* (23) and *C. glabrata* (25) clinical isolates harboring *erg6* mutations, indicating that cholesta-type sterols are a viable alternative to ergosterol. Although *M. circinelloides erg6a*Δ mutants exhibit minor defects in virulence, they can sustain mammalian physiological temperatures and effectively disseminate the infection. It is likely that the residual Erg6 activity observed in the *erg6a*Δ mutants can rescue the most deleterious consequences of loss of Erg6 function, while still conferring amphotericin B resistance due to cholesta-type sterols production.

In light of our findings, it is perplexing that a contemporary study of *M. lusitanicus erg6* mutants proposed that the fungus utilizes cholesta-type sterols to produce desmosterol or cholesterol (71), as this would require DHCR7 activity. Neither their analysis nor ours identified any C7-saturated sterols and although many EDF harbor DHCR7, mucoralean genomes do not encode this enzyme (62). Notably, the authors observed no changes in susceptibility to amphotericin B in their reported *erg6a* mutants, whereas we identified clear resistance to amphotericin B in multiple independently generated *erg6a*Δ mutants of two different *Mucor* species. We attribute these seemingly contradictory findings to potential methodological issues of gene deletion verification. Bauer et al. presented no DNA-based evidence confirming 1) the complete and homokaryotic deletion of *erg6* gene sequences, or 2) excluding ectopic integration or potential partial deletions, insertions, or off-target mutations due to non-homologous end joining DNA repair mechanisms that may be induced by Cas9 activity. Our findings are substantiated by a robust and rigorous molecular and genetic methodology, defining the most plausible pathway for the production

of cholesta-type sterols and their role in conferring amphotericin B resistance in *Mucor erg6a*Δ mutants, which is supported by research in other fungal pathogens.

Given the growing susceptible patient population and dearth of available antifungal drugs, mucormycoses pose substantial challenges to global public health. We propose that mutations and epimutations leading to the loss of Erg6a function may confer a selective advantage to Mucorales, allowing them to overcome amphotericin B treatment. Loss of Erg6a function may arise in vivo and lead to mucormycosis infections that do not respond to first-line antifungal therapies, and may challenge recent and exciting developments in polyene antifungal drug discovery (72). Currently, it is complicated to identify resistant clinical isolates because there are no clinical breakpoints defined for antifungal susceptibility testing in Mucorales species (73). Therefore, improving current guidelines to identify clinically amphotericin B-resistant isolates from mucormycosis patients should be a priority. Antifungal susceptibility testing may pose a challenge in identifying epimutant clinical isolates due to the transient and unstable nature of epigenetic changes, which can occur but remain undetected. This adds an additional layer of complexity to the identification of resistant clinical isolates but opens new and exciting avenues for future research.

Materials and methods

Fungal strains and culturing conditions. *M. lusitanicus* mutant strains generated in this work originate from the *M. lusitanicus* CBS277.49 strain. Its derivative, double auxotrophic (Ura-, Leu-) MU402 strain (74) was used as recipient for genetic transformation procedures, using the selectable marker *pyrG* to complement uracil auxotrophy. The MU636 strain (35) was used as the wildtype, complemented control (*pyrG*$^-$::*pyrG*$^+$ *leuA*$^-$) for phenotypic screening of *M. lusitanicus* mutants. Similarly, *M. circinelloides* mutant strains derive from *M. circinelloides* 1006PhL (39). A uracil auxotroph amenable to genetic transformation, MIN6 (Ura-) was generated in this work. Uridine auxotrophy was complemented by the selectable marker *pyrF*. All the strains generated in this study are listed in Table S3.

The growth rate of *erg3* and *erg6a* mutants was quantified by spot inoculating 500 spores onto rich yeast-peptone-dextrose (YPD) medium and minimal yeast-nitrogen-base (YNB) medium at 26 °C, 30 °C, and 37 °C. Images were taken every 24 hours for 3 days, and analyzed with Fiji (75) to determine the area of growth.

Isolation of uracil auxotrophic strain MIN6. 10^6 spores of the wildtype 1006PhL strain were spread-plated on YPD medium containing 5-FOA (3 g/L) supplemented with uracil (100 mg/L) and uridine (200 mg/L) and screened for resistant isolates after 3 days. Spores from resistant colonies were inoculated onto the same medium for a complete vegetative cycle, i.e. germination, colony formation, and asexual sporangiophore development (4-6 days). Colonies exhibiting stable 5-FOA resistance were inoculated onto YNB media with or without uracil and uridine as aforementioned to determine uracil auxotrophy. Genomic DNA from isolates that exhibited uracil auxotrophy was purified using the MasterPure™ Complete DNA and RNA Purification Kit (Lucigen). The promoter, ORF, and terminator containing sequences from *pyrG* and *pyrF* were PCR-amplified and Sanger-sequenced using primers listed in Table S4.

Protoplast generation and genetic transformation by electroporation. Protoplast generation and transformation by electroporation of *M. lusitanicus* was performed following previously established protocols (48). For *M. circinelloides* transformation, batches of 1.25 x 10^8 MIN6 spores were incubated in 25 mL of yeast-peptone-glucose (YPG) medium at 26 °C for 4 to 4.5 hours, specifically until germlings appeared. Cell walls were digested with a 0.01 M sodium phosphate buffer and 0.5 M sorbitol solution (48) containing 5 mg of lysing enzymes from *Trichoderma harzianum* (L-1412, Sigma-Aldrich) and 0.3 µL (15 U/mg) of chitosanase (C-0794, Sigma-Aldrich) at 30 °C for 1.5 hours, ensuring gentle shaking to avoid protoplast lethality. Protoplasts were washed with cold 0.5 M sorbitol solution, centrifuged at low speed ($\leq$ 1,000 rpm), and resuspended in 800 µL of 0.5 M sorbitol. After that, 200 µl of protoplasts were distributed into electroporation cuvettes, mixed with linear DNA (3-6 µg) and subjected to exponential decay waveform electroporation. Electroporation parameters were set to a field strength of 1,000 V ($E = 5kv \cdot cm^{-1}$), capacitance of 25 µF, and constant resistance of 400 Ω. Following electroporation, protoplasts were recovered in 1 mL of YPG medium, incubated at 26 °C for 1 hour, and spread-plated on minimal medium with casamino acids for *Mucor* (MMC) pH = 3.2 to select prototroph transformants after 2-5 days incubation in dark conditions.

For the deletion of *erg* genes in *M. lusitanicus* we designed a linear DNA construct containing the selectable marker *pyrG* flanked by 1-kb upstream and downstream regions of either the *erg3* or *erg6a* gene. For *M. circinelloides*, the linear DNA construct was similar but contained the selectable marker *pyrF*. In addition, a linear DNA fragment containing the wildtype *pyrF* marker sequence was used to transform MIN6 (*pyrF*-Δ59) and replace the *pyrF* mutated allele. This allowed us to 1) determine transformation efficiencies at a range of voltages and select the optimum to conduct subsequent electroporation experiments, and 2) generate a complemented control named CPA6 (*pyrF*-Δ59::*pyrF*$^+$). Gene replacements or deletions through integration by homologous recombination of the DNA cassette as well as homokaryosis were verified by PCR-amplification using primers that generate discriminatory amplicons (AFLP); first, transformants were analyzed after two vegetative passages in selective medium MMC, and subsequently, after every additional passage until homokaryosis was achieved.

Ortholog search and phylogenetic tree inference. Erg3 and Erg6 protein sequences from *Saccharomyces cerevisiae* were used as queries in a PSI-BLAST v2.12.0 search (76) against a proteomic database encompassing 13 mucoralean species known to cause animal or plant disease, the chytrid *Spizellomyces punctatus* as an outgroup, as well as four well-

known fungal pathogens that harbored *erg3* and *erg6* single copy genes, *Schizosaccharomyces pombe* and *S. cerevisiae* (see Table S5 for a comprehensive list of species and proteomes) (37–39, 45–47, 77–89). The glomeromycete *Rhizophagus irregularis* Erg6 homologs were also identified to clarify the phylogenetic inference. After that, every match was subjected to a reciprocal BLASTp search against the *S. cerevisiae* proteome, and positive reciprocal hits were retrieved. These putative orthologs (Tables S1 and S2) were aligned using MAFFT v7.475 (90), the resulting alignments were trimmed with TrimAl v1.4.rev15 gappyout method (91), and phylogenetic trees with 1,000 ultrafast bootstraps and SH-aLRT replicates were inferred from these alignment blocks by IQ-TREE v2.2.0.3 (92), detecting the best substitution models automatically.

RNA isolation, sequencing, and data analysis. 2.5 x 10^5 spore/mL YPD cultures were grown for 16 hours at 26 °C and 250 rpm in duplicates. Total RNA was purified with a QIAGEN miRNeasy Mini Kit. rRNA-depleted RNA libraries were prepared using Illumina Stranded Total RNA Prep with Ribo-Zero Gold rRNA Removal Kit and *M. circinelloides* rDNA specific probes, and cDNA sequenced in a NovaSeq 6000 sequencing system to obtain 150-bp paired-end reads. In addition to these, *M. lusitanicus* similar and publicly available rRNA-depleted RNA sequencing reads were used for gene expression analyses (57). FASTQ dataset quality was assessed by FASTQC v0.11.9 and reads processed by TrimGalore! V0.6.7 to remove adapters and low-quality reads. Processed reads were aligned to either *M. circinelloides* 1006PhL (https://fungidb.org/fungidb/app/record/dataset/DS_8b08c1c31d) or *M. lusitanicus* MU402 genome (https://mycocosm.jgi.doe.gov/Muccir1_3/Muccir1_3.info.html) employing STAR v.2.7.10a (93). Alignments were sorted and classified into forward and reverse stranded by Samtools sort, view, and merge according to their flag values as follows: forward alignments included first-pair alignments from the reverse strand (-f 64 and 16) and second-pair alignments excluding those from the reverse strand (-f 128 and -F 16), and reverse alignments included second-pair alignments from the reverse strand (-f 128 and 16) and first-pair alignments excluding those from the reverse strand (-f 64 and -F 16). Then, coverage files were generated using bamCompare from Deeptools2 v3.5.1 (94) to merge duplicates into a single bigWig file.

Synteny analysis. Pairwise synteny among closely related mucoralean species was assessed at the amino acid level using the JCVI toolkit MCScan pipeline (95), defining synteny range to a maximum of 30 kilobases and a minimum of 2 anchors per cluster. Genomic plots were generated by Deeptools2 pyGenomeTracks v3.7 (96) and protein synteny was manually annotated as pink Bezier curves between species. Genes were plotted as single blocks, i.e. ignoring intron-exon information to facilitate rendering and visualization.

Virulence and fungal burden assays. 4-week old BALB/c mice (Charles River) weighing approximately 20 to 25 g were used as a host model for virulence assays. Mice were immunosuppressed with cyclophosphamide via intraperitoneal injection (200 mg/kg of body weight), 2 days prior to infection and every 5 days thereafter. Groups of 10 mice were intravenously challenged via retro-orbital injection with 1 x 10^6 spores from each of the mutant and control strains. Survival and disease symptomatology of each group of mice were monitored every 12 hours, and animals meeting end-point criteria were euthanized by CO_2 inhalation and a secondary method.

Fungal burden was quantified in three infected mice meeting end-point criteria per group. Animals were dissected to extract five organs (brain, lung, spleen, kidney, and liver), which were homogenized. Organ homogenates were plated on YPD media supplemented with 1 μg/mL of FK506 to induce yeast growth and were incubated for 4 days. Colony forming units (CFU) were quantified and normalized per volume plated and organ weight.

Antifungal drug susceptibility testing. Antifungal drug susceptibility profiles were determined by broth microdilution using the CLSI and EUCAST standard methodology for molds. Briefly, minimal inhibitory concentrations required to inhibit visible growth by eye (MIC) were evaluated for amphotericin B, posaconazole, and isavuconazole. 10^5 spores/mL were incubated in Roswell Park Memorial Institute (RPMI) 1640 medium with each drug at 35 °C for 24 and 48 hours. Results were read visually and wells evaluated for visible growth or lack therein. Additionally, 500 spores were spot-inoculated onto YPD solid medium containing drugs at defined concentrations: 8 mg/L of liposomal amphotericin B (Ambisome, Gilead Sciences), 0.2 mg/L of posaconazole (Noxafil, Merck), and 8 mg/L of isavuconazole (Cresemba, Astellas Pharma). Images of growth were taken at 24-hour intervals, and analyzed with Fiji to measure the area of growth. The area of inhibited growth was determined as the ratio of growth area in treated compared to untreated plates.

Ergosterol profile quantification. Non-saponifiable lipids were extracted from lyophilized mycelia as previously described (12), with cholesterol added as an internal standard. Sterols were derivatized using 0.1 mL *N,O*-Bis(trimethylsilyl)trifluoroacetamide and trimethylsilyl chloride [BSTFA and TMCS, (99:1)] and 0.3 mL anhydrous pyridine and heating at 80 °C for 2 hours (97). TMS-derivatized sterols were analyzed using gas chromatography–mass spectrometry (GS/MS) (Thermo 1300 GC coupled to a Thermo ISQ mass spectrometer, Thermo Scientific) and identified with reference to relative retention times, mass ions and fragmentation spectra. GC/MS data files were analyzed using Xcalibur software (Thermo Scientific). Sterol composition was calculated from peak areas, as a mean of 3 replicates per independently generated mutant (6 replicates per gene deletion) or 6 replicates for the wildtype strain 1006PhL. The relative quantity of sterols present was determined from the peak areas of the sterol and the internal standard and divided by the dry weight of the sample.

Data availability. Raw rRNA-depleted RNA-sequencing datasets obtained from the *M. circinelloides* 1006PhL strain will be accessible upon publication under the following

NCBI's Sequence Read Archive (SRA) project accession number: PRJNA1046487. RNA-seq datasets derived from the *M. lusitanicus* MU402 strain were similarly generated for a prior study (57) and are publicly available, assigned to the NCBI's SRA project accession number: PRJNA903107.

ACKNOWLEDGEMENTS

We thank Anna Floyd Averette for her constant technical support. We also extend our gratitude to Marcus Hull for providing technical support during the ergosterol profiling process. We commend Dr. Devjanee Swain Lenz and Duke's Sequencing and Genomic Technologies Core Facility for their assistance, as well as Thomas Milledge and the Duke Computer Cluster team for their computing resources. This study was supported by Astellas Pharma Investigator Sponsored Research ISR005855/CRES-21B01, and NIH/National Institute of Allergy and Infectious Diseases R01 Grant R01 AI170543 both awarded to J.H. The funders had no role in study design, data collection and interpretation, or the decision to submit the work for publication. J.H. is Codirector and Fellow of the CIFAR program Fungal Kingdom: Threats & Opportunities.

References

1. G. Petrikkos, A. Skiada, O. Lortholary, E. Roilides, T. J. Walsh, and D. P. Kontoyiannis. Epidemiology and clinical manifestations of mucormycosis. *Clinical Infectious Diseases*, 54 (1):23–34, 2012. doi: 10.1093/cid.cir866.
2. O. A. Cornely, A. Alastruey-Izquierdo, D. Arenz, S. C. A. Chen, E. Dannaoui, B. Hochhegger, M. Hoenigl, H. E. Jensen, K. Lagrou, R. E. Lewis, S. C. Mellinghoff, M. Mer, Z. D. Pana, D. Seidel, D. C. Sheppard, R. Wahba, M. Akova, A. Alanio, A. M. S. Al-Hatmi, S. Arikan-Akdagli, H. Badali, R. Ben-Ami, A. Bonifaz, S. Bretagne, E. Castagnola, M. Chayakulkeeree, A. L. Colombo, D. E. Corzo-León, L. Drgona, A. H. Groll, J. Guinea, C.-P. Heussel, A. S. Ibrahim, S. S. Kanj, N. Klimko, M. Lackner, F. Lamoth, F. Lanternier, C. Lass-Floerl, D.-G. Lee, T. Lehrnbecher, B. E. Lmimouni, M. Mares, G. Maschmeyer, J. F. Meis, J. Meletiadis, C. O. Morrissey, M. Nucci, R. Oladele, L. Pagano, A. Pasqualotto, A. Patel, Z. Racil, M. Richardson, E. Roilides, M. Ruhnke, S. Seyedmousavi, N. Sidharthan, N. Singh, J. Sinko, A. Skiada, M. Slavin, R. Soman, B. Spellberg, W. Steinbach, B. H. Tan, A. J. Ullmann, J. J. Vehreschild, M. J. G. T. Vehreschild, T. J. Walsh, P. L. White, N. P. Wiederhold, T. Zaoutis, and A. Chakrabarti. Global guideline for the diagnosis and management of mucormycosis: an initiative of the European Confederation of Medical Mycology in cooperation with the Mycoses Study Group Education and Research Consortium. *The Lancet Infectious Diseases*, 19(12):e405–e421, 2019. doi: 10.1016/S1473-3099(19)30312-3.
3. M. Hoenigl, D. Seidel, A. Carvalho, S. M. Rudramurthy, A. Arastehfar, J.-P. Gangneux, N. Nasir, A. Bonifaz, J. Araiza, N. Klimko, A. Serris, K. Lagrou, J. F. Meis, O. A. Cornely, J. R. Perfect, P. L. White, and A. Chakrabarti. The emergence of COVID-19 associated mucormycosis: a review of cases from 18 countries. *The Lancet Microbe*, 3(7):e543–e552, 2022. doi: 10.1016/S2666-5247(21)00237-8.
4. J. A. Gold, S. Adjei, A. V. Gundlapalli, Y.-L. A. Huang, T. Chiller, K. Benedict, and M. Toda. Increased hospitalizations involving fungal infections during COVID-19 pandemic, United States, January 2020–December 2021. *Emerging Infectious Diseases*, 29(7):1433–1437, 2023. doi: 10.3201/eid2907.221771.
5. Geneva: World Health Organization. *WHO fungal priority pathogens list to guide research, development and public health action*. World Health Organization, cc by-nc-sa 3.0 igo edition, 2022. ISBN 978-92-4-006024-1.
6. R. Caramalho, J. D. Tyndall, B. C. Monk, T. Larentis, C. Lass-Flörl, and M. Lackner. Intrinsic short-tailed azole resistance in mucormycetes is due to an evolutionary conserved aminoacid substitution of the lanosterol 14α-demethylase. *Scientific Reports*, 7(1):3–12, 2017. doi: 10.1038/s41598-017-16123-9.
7. N. G. Almyroudis, D. A. Sutton, A. W. Fothergill, M. G. Rinaldi, and S. Kusne. In vitro susceptibilities of 217 clinical isolates of zygomycetes to conventional and new antifungal agents. *Antimicrobial Agents and Chemotherapy*, 51(7):2587–90, 2007. doi: 10.1128/AAC.00452-07.
8. S. Calo, C. Shertz-Wall, S. C. Lee, R. J. Bastidas, F. E. Nicolás, J. A. Granek, P. Mieczkowski, S. Torres-Martínez, R. M. Ruiz-Vázquez, M. E. Cardenas, and J. Heitman. Antifungal drug resistance evoked via RNAi-dependent epimutations. *Nature*, 513:555–558, 2014. doi: 10.1038/nature13575.
9. Z. Chang and J. Heitman. Drug-resistant epimutants exhibit organ-specific stability and induction during murine infections caused by the human fungal pathogen *Mucor circinelloides*. *mBio*, 10(6):e02579–19, 2019. doi: 10.1128/mBio.02579-19.
10. D. S. Palacios, I. Dailey, D. M. Siebert, B. C. Wilcock, and M. D. Burke. Synthesis-enabled functional group deletions reveal key underpinnings of amphotericin B ion channel and antifungal activities. *Proceedings of the National Academy of Sciences*, 108(17):6733–8, 2011. doi: 10.1073/pnas.1015023108.
11. K. C. Gray, D. S. Palacios, I. Dailey, M. M. Endo, B. E. Uno, B. C. Wilcock, and M. D. Burke. Amphotericin primarily kills yeast by simply binding ergosterol. *Proceedings of the National Academy of Sciences*, 109(7):2234–9, 2012. doi: 10.1073/pnas.1117280109.
12. S. L. Kelly, D. C. Lamb, A. J. Corran, B. C. Baldwin, and D. E. Kelly. Mode of action and resistance to azole antifungals associated with the formation of 14 alpha-methylergosta-8,24(28)-dien-3 beta,6 alpha-diol. *Biochemical and Biophysical Research Communications*, 207(3):910–5, 1995. doi: 10.1006/bbrc.1995.1272.
13. P. F. Watson, M. E. Rose, S. W. Ellis, H. England, and S. L. Kelly. Defective sterol C5-6 desaturation and azole resistance: a new hypothesis for the mode of action of azole antifungals. *Biochemical and Biophysical Research Communications*, 164(3):1170–5, 1989. doi: 10.1016/0006-291x(89)91792-0.
14. J. E. Parker, A. G. S. Warrilow, C. L. Price, J. G. L. Mullins, D. E. Kelly, and S. L. Kelly. Resistance to antifungals that target CYP51. *Journal of Chemical Biology*, 7(4):143–161, 2014. doi: 10.1007/s12154-014-0121-1.
15. C. M. Martel, J. E. Parker, O. Bader, M. Weig, U. Gross, A. G. S. Warrilow, N. Rolley, D. E. Kelly, and S. L. Kelly. Identification and characterization of four azole-resistant *erg3* mutants of *Candida albicans*. *Antimicrobial Agents and Chemotherapy*, 54(11):4527–33, 2010. doi: 10.1128/AAC.00348-10.
16. S. L. Kelly, D. C. Lamb, D. E. Kelly, N. J. Manning, J. Loeffler, H. Hebart, U. Schumacher, and H. Einsele. Resistance to fluconazole and cross-resistance to amphotericin B in *Candida albicans* from AIDS patients caused by defective sterol delta5,6-desaturation. *FEBS Letters*, 400(1):80–2, 1997. doi: 10.1016/s0014-5793(96)01360-9.
17. L. A. Vale-Silva, A. T. Coste, F. Ischer, J. E. Parker, S. L. Kelly, E. Pinto, and D. Sanglard. Azole resistance by loss of function of the sterol $\Delta^{5,6}$-desaturase gene (*ERG3*) in *Candida albicans* does not necessarily decrease virulence. *Antimicrobial Agents and Chemotherapy*, 56(4):1960–8, 2012. doi: 10.1128/AAC.05720-11.
18. J. M. Rybak, C. M. Dickens, J. E. Parker, K. E. Caudle, K. Manigaba, S. G. Whaley, A. T. Nishimoto, A. Luna-Tapia, S. Roy, Q. Zhang, K. S. Barker, G. E. Palmer, T. R. Sutter, R. Homayouni, N. P. Wiederhold, S. L. Kelly, and P. D. Rogers. Loss of C-5 sterol desaturase activity results in increased resistance to azole and echinocandin antifungals in a clinical isolate of *Candida parapsilosis*. *Antimicrobial Agents and Chemotherapy*, 61(9): e00651–17, 2017. doi: 10.1128/AAC.00651-17.
19. E. Ksiezopolska, M. À. Schikora-Tamarit, R. Beyer, J. C. Nunez-Rodriguez, C. Schüller, and T. Gabaldón. Narrow mutational signatures drive acquisition of multidrug resistance in the fungal pathogen *Candida glabrata*. *Current Biology*, 31(23):5314–5326, 2021. doi: 10.1016/j.cub.2021.09.084.
20. N. E. Scott, S. Edwin Erayil, S. E. Kline, and A. Selmecki. Rapid evolution of multidrug resistance in a *Candida lusitaniae* infection during micafungin monotherapy. *Antimicrobial Agents and Chemotherapy*, 67(8):e0054323, 2023. doi: 10.1128/aac.00543-23.
21. M. T. McCammon, M. A. Hartmann, C. D. Bottema, and L. W. Parks. Sterol methylation in *Saccharomyces cerevisiae*. *Journal of Bacteriology*, 157(2):475–83, 1984. doi: 10.1128/jb.157.2.475-483.1984.
22. K. L. Jensen-Pergakes, M. A. Kennedy, N. D. Lees, R. Barbuch, C. Koegel, and M. Bard. Sequencing, disruption, and characterization of the *Candida albicans* sterol methyltransferase (*ERG6*) gene: drug susceptibility studies in *erg6* mutants. *Antimicrobial Agents and Chemotherapy*, 42(5):1160–1167, 1998. doi: 10.1128/AAC.42.5.1160.
23. J. M. Rybak, K. S. Barker, J. F. Muñoz, J. E. Parker, S. Ahmad, E. Mokaddas, A. Abdullah, R. S. Elhagracy, S. L. Kelly, C. A. Cuomo, and P. D. Rogers. In vivo emergence of high-level resistance during treatment reveals the first identified mechanism of amphotericin B resistance in *Candida auris*. *Clinical Microbiology and Infection*, 28(6):838–843, 2022. doi: 10.1016/j.cmi.2021.11.024.
24. L. Y. Young, C. M. Hull, and J. Heitman. Disruption of ergosterol biosynthesis confers resistance to amphotericin B in *Candida lusitaniae*. *Antimicrobial Agents and Chemotherapy*, 47 (9):2717–24, 2003. doi: 10.1128/aac.47.9.2717-2724.2003.
25. S. Ahmad, L. Joseph, J. E. Parker, M. Asadzadeh, S. L. Kelly, J. F. Meis, and Z. Khan. *ERG6* and *ERG2* are major targets conferring reduced susceptibility to amphotericin B in clinical *Candida glabrata* isolates in Kuwait. *Antimicrobial Agents and Chemotherapy*, 63 (2):e01900–18, 2019. doi: 10.1128/AAC.01900-18.
26. T. Joseph-Horne, D. Hollomon, R. S. Loeffler, and S. L. Kelly. Cross-resistance to polyene and azole drugs in *Cryptococcus neoformans*. *Antimicrobial Agents and Chemotherapy*, 39 (7):1526–9, 1995. doi: 10.1128/AAC.39.7.1526.
27. F. F. M. Oliveira, H. C. Paes, L. D. F. Peconick, F. L. Fonseca, C. L. F. Marina, A. L. Bocca, M. Homem-de Mello, M. L. Rodrigues, P. Albuquerque, A. M. Nicola, J. A. Alspaugh, M. S. S. Felipe, and L. Fernandes. Erg6 affects membrane composition and virulence of the human fungal pathogen *Cryptococcus neoformans*. *Fungal Genetics and Biology*, 140:103368, 2020. doi: 10.1016/j.fgb.2020.103368.
28. P. Vandeputte, G. Tronchin, G. Larcher, E. Ernoult, T. Bergès, D. Chabasse, and J.-P. Bouchara. A nonsense mutation in the *ERG6* gene leads to reduced susceptibility to polyenes in a clinical isolate of *Candida glabrata*. *Antimicrobial Agents and Chemotherapy*, 52(10):3701–9, 2008. doi: 10.1128/AAC.00423-08.
29. L. Wagner, J. B. Stielow, G. S. de Hoog, K. Bensch, V. U. Schwartze, K. Voigt, A. Alastruey-Izquierdo, O. Kurzai, and G. Walther. A new species concept for the clinically relevant *Mucor circinelloides* complex. *Persoonia*, 44:67–97, 2020. doi: 10.3767/persoonia.2020.44.03.
30. M. Richardson. The ecology of the Zygomycetes and its impact on environmental exposure. *Clinical Microbiology and Infection*, 15(5):2–9, 2009. doi: 10.1111/j.1469-0691.2009.02972.x.
31. G. Walther, J. Pawłowska, A. Alastruey-Izquierdo, M. Wrzosek, J. L. Rodriguez-Tudela, S. Dolatabadi, A. Chakrabarti, and G. S. de Hoog. DNA barcoding in Mucorales: an inventory of biodiversity. *Persoonia*, 30:11–47, 2013. doi: 10.3767/003158513X665070.
32. B. Mousavi, J. M. Costa, P. Arné, J. Guillot, R. Chermette, F. Botterel, and E. Dannaoui. Occurrence and species distribution of pathogenic Mucorales in unselected soil samples from France. *Medical Mycology*, 56(3):315–321, 2018. doi: 10.1093/mmy/myx051.
33. S. C. Lee, A. Li, S. Calo, and J. Heitman. Calcineurin plays key roles in the dimorphic transition and virulence of the human pathogenic zygomycete *Mucor circinelloides*. *PLoS Pathogens*, 9(9):e1003625, 2013. doi: 10.1371/journal.ppat.1003625.
34. M. I. Navarro-Mendoza, C. Pérez-Arques, L. Murcia, P. Martínez-García, C. Lax, M. Sanchis, J. Capilla, F. E. Nicolás, and V. Garre. Components of a new gene family of ferroxidases involved in virulence are functionally specialized in fungal dimorphism. *Scientific Reports*, 8 (1):7660, 2018. doi: 10.1038/s41598-018-26051-x.
35. C. Pérez-Arques, M. I. Navarro-Mendoza, L. Murcia, C. Lax, P. Martínez-García, J. Heitman, F. E. Nicolás, and V. Garre. *Mucor circinelloides* thrives inside the phagosome through an Atf-mediated germination pathway. *mBio*, 10(1):1–15, 2019. doi: 10.1128/mBio.02765-18.
36. C. Pérez-Arques, M. I. Navarro-Mendoza, L. Murcia, E. Navarro, V. Garre, and F. E. Nicolás. A non-canonical RNAi pathway controls virulence and genome stability in Mucorales. *PLoS Genetics*, 16(7):e1008611, 2020. doi: 10.1371/journal.pgen.1008611.
37. L. M. Corrochano, A. Kuo, M. Marcet-Houben, S. Polaino, A. Salamov, J. M. Villalobos-Escobedo, J. Grimwood, M. I. Álvarez, J. Avalos, D. Bauer, E. P. Benito, I. Benoit, G. Burger, L. P. Camino, D. Cánovas, E. Cerdá-Olmedo, J. F. Cheng, A. Domínguez, M. Eliáš, A. P.

Eslava, F. Glaser, G. Gutiérrez, J. Heitman, B. Henrissat, E. A. Iturriaga, B. F. Lang, J. L. Lavín, S. C. Lee, W. Li, E. Lindquist, S. López-García, E. M. Luque, A. T. Marcos, J. Martin, K. McCluskey, H. R. Medina, A. Miralles-Durán, A. Miyazaki, E. Muñoz-Torres, J. A. Oguiza, R. A. Ohm, M. Olmedo, M. Orejas, L. Ortiz-Castellanos, A. G. Pisabarro, J. Rodríguez-Romero, J. Ruiz-Herrera, R. Ruiz-Vázquez, C. Sanz, W. Schackwitz, M. Shahriari, E. Shelest, F. Silva-Franco, D. Soanes, K. Syed, V. G. Tagua, N. J. Talbot, M. R. Thon, H. Tice, R. P. de Vries, A. Wiebenga, J. S. Yadav, E. L. Braun, S. E. Baker, V. Garre, J. Schmutz, B. A. Horwitz, S. Torres-Martínez, A. Idnurm, A. Herrera-Estrella, T. Gabaldón, and I. V. Grigoriev. Expansion of signal transduction pathways in fungi by extensive genome duplication. *Current Biology*, 26(12):1577–1584, 2016. doi: 10.1016/j.cub.2016.04.038.

38. M. I. Navarro-Mendoza, C. Pérez-Arques, S. Panchal, F. E. Nicolás, S. J. Mondo, P. Ganguly, J. Pangilinan, I. V. Grigoriev, J. Heitman, K. Sanyal, and V. Garre. Early diverging fungus *Mucor circinelloides* lacks centromeric histone CENP-A and displays a mosaic of point and regional centromeres. *Current Biology*, 29(22):3791–3802, 2019. doi: 10.1016/j.cub.2019.09.024.
39. K. Findley, J. Oh, J. Yang, S. Conlan, C. Deming, J. A. Meyer, D. Schoenfeld, E. Nomicos, M. Park, NIH Intramural Sequencing Center Comparative Sequencing Program, H. H. Kong, and J. A. Segre. Topographic diversity of fungal and bacterial communities in human skin. *Nature*, 498:367–70, 2013. doi: 10.1038/nature12171.
40. S. C. Lee, R. B. Billmyre, A. Li, S. Carson, S. M. Sykes, E. Y. Huh, P. Mieczkowski, D. C. Ko, C. A. Cuomo, and J. Heitman. Analysis of a food-borne fungal pathogen outbreak: virulence and genome of a *Mucor circinelloides* isolate from yogurt. *mBio*, 5(4):e01390–14, 2014. doi: 10.1128/mBio.01390-14.
41. C. Lax, M. I. Navarro-Mendoza, C. Pérez-Arques, E. Navarro, F. E. Nicolás, and V. Garre. Stable and reproducible homologous recombination enables CRISPR-based engineering in the fungus *Rhizopus microsporus*. *Cell Reports Methods*, 1(8):100124, 2021. doi: 10.1016/j.crmeth.2021.100124.
42. C. H. Li, M. Cervantes, D. J. Springer, T. Boekhout, R. M. Ruiz-Vazquez, S. R. Torres-Martinez, J. Heitman, and S. C. Lee. Sporangiospore size dimorphism is linked to virulence of *Mucor circinelloides*. *PLoS Pathogens*, 7(6):e1002086, 2011. doi: 10.1371/journal.ppat.1002086.
43. A. Lupetti, R. Danesi, M. Campa, M. Del Tacca, and S. Kelly. Molecular basis of resistance to azole antifungals. *Trends in Molecular Medicine*, 8(2):76–81, 2002. doi: 10.1016/s1471-4914(02)02280-3.
44. N. Robbins, T. Caplan, and L. E. Cowen. Molecular evolution of antifungal drug resistance. *Annual Review of Microbiology*, 71(1):753–775, 2017. doi: 10.1146/annurev-micro-030117-020345.
45. V. U. Schwartze, S. Winter, E. Shelest, M. Marcet-Houben, F. Horn, S. Wehner, J. Linde, V. Valiante, M. Sammeth, K. Riege, M. Nowrousian, K. Kaerger, I. D. Jacobsen, M. Marz, A. A. Brakhage, T. Gabaldón, S. Böcker, and K. Voigt. Gene expansion shapes genome architecture in the human pathogen *Lichtheimia corymbifera*: an evolutionary genomics analysis in the ancient terrestrial Mucorales (Mucoromycotina). *PLoS Genetics*, 10(8):e1004496, 2014. doi: 10.1371/journal.pgen.1004496.
46. L.-J. Ma, A. S. Ibrahim, C. Skory, M. G. Grabherr, G. Burger, M. Butler, M. Elias, A. Idnurm, B. F. Lang, T. Sone, A. Abe, S. E. Calvo, L. M. Corrochano, R. Engels, J. Fu, W. Hansberg, J.-M. Kim, C. D. Kodira, M. J. Koehrsen, B. Liu, D. Miranda-Saavedra, S. O'Leary, L. Ortiz-Castellanos, R. Poulter, J. Rodriguez-Romero, J. Ruiz-Herrera, Y.-Q. Shen, Q. Zeng, J. Galagan, B. W. Birren, C. A. Cuomo, and B. L. Wickes. Genomic analysis of the basal lineage fungus *Rhizopus oryzae* reveals a whole-genome duplication. *PLoS Genetics*, 5(7):e1000549, 2009. doi: 10.1371/journal.pgen.1000549.
47. A. P. Gryganskyi, J. Golan, S. Dolatabadi, S. Mondo, S. Robb, A. Idnurm, A. Muszewska, K. Steczkiewicz, S. Masonjones, H.-L. Liao, M. T. Gajdeczka, F. Anike, A. Vuek, I. M. Anishchenko, K. Voigt, G. S. de Hoog, M. E. Smith, J. Heitman, R. Vilgalys, and J. E. Stajich. Phylogenetic and phylogenomic definition of *Rhizopus* species. *G3*, 8(6):2007–2018, 2018. doi: 10.1534/g3.118.200235.
48. F. Nicolás, M. Navarro-Mendoza, C. Pérez-Arques, S. López-García, E. Navarro, S. Torres-Martínez, and V. Garre. Molecular tools for carotenogenesis analysis in the mucoral *Mucor circinelloides*. In C. Barreiro and J. L. Barredo, editors, *Microbial Carotenoids. Methods in Molecular Biology*, volume 1852. Humana Press, New York, NY, 2018. doi: 10.1007/978-1-4939-8742-9_13.
49. A. Luna-Tapia, J. E. Parker, S. L. Kelly, and G. E. Palmer. Species-specific differences in C-5 sterol desaturase function influence the outcome of azole antifungal exposure. *Antimicrobial Agents and Chemotherapy*, 65(12):e0104421, 2021. doi: 10.1128/aac.01044-21.
50. J. Xie, J. M. Rybak, A. Martin-Vicente, X. Guruceaga, H. I. Thorn, A. V. Nywening, W. Ge, J. E. Parker, S. L. Kelly, P. D. Rogers, and J. R. Fortwendel. The sterol C-24 methyltransferase encoding gene, *erg6*, is essential for viability of *Aspergillus* species. *bioRxiv*, 2023. doi: 10.1101/2023.08.08.552489.
51. L. Wagner, S. de Hoog, A. Alastruey-Izquierdo, K. Voigt, O. Kurzai, and G. Walther. A revised species concept for opportunistic *Mucor* species reveals species-specific antifungal susceptibility profiles. *Antimicrobial Agents and Chemotherapy*, 63(8):1–8, 2019. doi: 10.1128/AAC.00653-19.
52. F. E. Nicolás, L. Murcia, E. Navarro, M. I. Navarro-Mendoza, C. Pérez-Arques, and V. Garre. Mucorales species and macrophages. *Journal of Fungi*, 6(2):94, 2020. doi: 10.3390/jof6020094.
53. A. Varma, J. C. Edman, and K. J. Kwon-Chung. Molecular and genetic analysis of *URA5* transformants of *Cryptococcus neoformans*. *Infection and Immunity*, 60(3):1101–1108, 1992. doi: 10.1128/iai.60.3.1101-1108.1992.
54. C. D'Enfert, M. Diaquin, A. Delit, N. Wuscher, J. P. Debeaupuis, M. Huerre, and J. P. Latge. Attenuated virulence of uridine-uracil auxotrophs of *Aspergillus fumigatus*. *Infection and Immunity*, 64(10):4401–5, 1996. doi: 10.1128/iai.64.10.4401-4405.1996.
55. D. M. Retallack, E. L. Heinecke, R. Gibbons, G. S. Deepe, and J. P. Woods. The *URA5* gene is necessary for *Histoplasma capsulatum* growth during infection of mouse and human cells. *Infection and Immunity*, 67(2):624–9, 1999. doi: 10.1128/IAI.67.2.624-629.1999.
56. M. C. Fisher, A. Alastruey-Izquierdo, J. Berman, T. Bicanic, E. M. Bignell, P. Bowyer, M. Bromley, R. Brüggemann, G. Garber, O. A. Cornely, S. J. Gurr, T. S. Harrison, E. Kuijper, J. Rhodes, D. C. Sheppard, A. Warris, P. L. White, J. Xu, B. Zwaan, and P. E. Verweij. Tackling the emerging threat of antifungal resistance to human health. *Nature reviews. Microbiology*, 20(9):557–571, 2022. doi: 10.1038/s41579-022-00720-1.
57. M. I. Navarro-Mendoza, C. Pérez-Arques, and J. Heitman. Heterochromatin and RNAi act independently to ensure genome stability in Mucorales human fungal pathogens. *Proceedings of the National Academy of Sciences*, 120(7):e2220475120, 2023. doi: 10.1073/pnas.2220475120.
58. S. Calo, F. E. Nicolás, S. C. Lee, A. Vila, M. Cervantes, S. Torres-Martínez, R. M. Ruiz-Vázquez, M. E. Cardenas, and J. Heitman. A non-canonical rna degradation pathway suppresses rnai-dependent epimutations in the human fungal pathogen *Mucor circinelloides*. *PLoS Genetics*, 13(3):e1006686, 2017. doi: 10.1371/journal.pgen.1006686.
59. W. D. Nes, W. Zhou, K. Ganapathy, J. Liu, R. Vatsyayan, S. Chamala, K. Hernandez, and M. Miranda. Sterol 24-C-methyltransferase: An enzymatic target for the disruption of ergosterol biosynthesis and homeostasis in *Cryptococcus neoformans*. *Archives of Biochemistry and Biophysics*, 481(2):210–218, 2009. doi: 10.1016/j.abb.2008.11.003.
60. S. Bhattacharya, B. D. Esquivel, and T. C. White. Overexpression or deletion of ergosterol biosynthesis genes alters doubling time, response to stress agents, and drug susceptibility in *Saccharomyces cerevisiae*. *mBio*, 9(4):e01291–18, 2018. doi: 10.1128/mBio.01291-18.
61. J. D. Weete, M. Abril, and M. Blackwell. Phylogenetic distribution of fungal sterols. *PLoS ONE*, 5(5):e10899, 2010. doi: 10.1371/journal.pone.0010899.
62. K. R. Amses, D. R. Simmons, J. E. Longcore, S. J. Mondo, K. Seto, G. H. Jerônimo, A. E. Bonds, C. A. Quandt, W. J. Davis, Y. Chang, B. A. Federici, A. Kuo, K. LaButti, J. Pangilinan, W. Andreopoulos, A. Tritt, R. Riley, H. Hundley, J. Johnson, A. Lipzen, K. Barry, B. F. Lang, C. A. Cuomo, N. E. Buchler, I. V. Grigoriev, J. W. Spatafora, J. E. Stajich, and T. Y. James. Diploid-dominant life cycles characterize the early evolution of Fungi. *Proceedings of the National Academy of Sciences*, 119(36):e2116841119, 2022. doi: 10.1073/pnas.2116841119.
63. C. M. Hull, J. E. Parker, O. Bader, M. Weig, U. Gross, A. G. S. Warrilow, D. E. Kelly, and S. L. Kelly. Facultative sterol uptake in an ergosterol-deficient clinical isolate of *Candida glabrata* harboring a missense mutation in *ERG11* and exhibiting cross-resistance to azoles and amphotericin B. *Antimicrobial Agents and Chemotherapy*, 56(8):4223–32, 2012. doi: 10.1128/AAC.06253-11.
64. D. Sanglard, F. Ischer, T. Parkinson, D. Falconer, and J. Bille. *Candida albicans* mutations in the ergosterol biosynthetic pathway and resistance to several antifungal agents. *Antimicrobial Agents and Chemotherapy*, 47(8):2404–2412, 2003. doi: 10.1128/AAC.47.8.2404-2412.2003.
65. C. Papp, F. Bohner, K. Kocsis, M. Varga, A. Szekeres, L. Bodai, J. R. Willis, T. Gabaldón, R. Tóth, J. D. Nosanchuk, C. Vágvölgyi, and A. Gácser. Triazole evolution of *Candida parapsilosis* results in cross-resistance to other antifungal drugs, influences stress responses, and alters virulence in an antifungal drug-dependent manner. *mSphere*, 5(5):e00821–20, 2020. doi: 10.1128/mSphere.00821-20.
66. A. S. Chau, M. Gurnani, R. Hawkinson, M. Laverdiere, A. Cacciapuoti, and P. M. McNicholas. Inactivation of sterol $\Delta^{5,6}$-desaturase attenuates virulence in *Candida albicans*. *Antimicrobial Agents and Chemotherapy*, 49(9):3646–3651, 2005. doi: 10.1128/AAC.49.9.3646-3651.2005.
67. F. Ben Abid, H. Salah, S. Sundararaju, L. Dalil, A. H. Abdelwahab, S. Salameh, E. B. Ibrahim, M. A. Almaslmani, P. Tang, A. Perez-Lopez, and C. K. Tsui. Molecular characterization of *Candida auris* outbreak isolates in Qatar from patients with COVID-19 reveals the emergence of isolates resistant to three classes of antifungal drugs. *Clinical Microbiology and Infection*, 29(8):1083.e1–1083.e7, 2023. doi: 10.1016/j.cmi.2023.04.025.
68. R. S. Shapiro, N. Robbins, and L. E. Cowen. Regulatory circuitry governing fungal development, drug resistance, and disease. *Microbiology and Molecular Biology Reviews*, 75(2):213–267, 2011. doi: 10.1128/MMBR.00045-10.
69. F. S. Nolte, T. Parkinson, D. J. Falconer, S. Dix, J. Williams, C. Gilmore, R. Geller, and J. R. Wingard. Isolation and characterization of fluconazole- and amphotericin B-resistant *Candida albicans* from blood of two patients with leukemia. *Antimicrobial Agents and Chemotherapy*, 41(1):196–9, 1997. doi: 10.1128/AAC.41.1.196.
70. N. Robbins and L. E. Cowen. Antifungal drug resistance: Deciphering the mechanisms governing multidrug resistance in the fungal pathogen *Candida glabrata*. *Current Biology*, 31(23):R1520–R1523, 2021. doi: 10.1016/j.cub.2021.09.071.
71. K. Bauer, B. Rafael, B. Vágó, S. Kiss-Vetráb, A. Molnár, C. Szebenyi, M. Varga, A. Szekeres, C. Vágvölgyi, T. Papp, and G. Nagy. Characterization of the sterol 24-C-methyltransferase genes reveals a network of alternative sterol biosynthetic pathways in *Mucor lusitanicus*. *Microbiology Spectrum*, 11(3):e0031523, 2023. doi: 10.1128/spectrum.00315-23.
72. A. Maji, C. P. Soutar, J. Zhang, A. Lewandowska, B. E. Uno, S. Yan, Y. Shelke, G. Murhade, E. Nimerovsky, C. G. Borcik, A. S. Arango, J. D. Lange, J. P. Marin-Toledo, Y. Lyu, K. L. Bailey, P. J. Roady, J. T. Holler, A. Khandelwal, A. M. SantaMaria, H. Sanchez, P. R. Juvvadi, G. Johns, M. J. Hageman, J. Krise, T. Gebremariam, E. G. Youssef, K. Bartizal, K. A. Marr, W. J. Steinbach, A. S. Ibrahim, T. F. Patterson, N. P. Wiederhold, D. R. Andes, T. V. Pogorelov, C. D. Schwieters, T. M. Fan, C. M. Rienstra, and M. D. Burke. Tuning sterol extraction kinetics yields a renal-sparing polyene antifungal. *Nature*, 623:1079–1085, 2023. doi: 10.1038/s41586-023-06710-4.
73. A. Espinel-Ingroff, A. Chakrabarti, A. Chowdhary, S. Cordoba, E. Dannaoui, P. Dufresne, A. Fothergill, M. Ghannoum, G. M. Gonzalez, J. Guarro, S. Kidd, C. Lass-Flörl, J. F. Meis, T. Pelaez, A. M. Tortorano, and J. Turnidge. Multicenter evaluation of MIC distributions for epidemiologic cutoff value definition to detect Amphotericin B, Posaconazole, and Itraconazole resistance among the most clinically relevant species of Mucorales. *Antimicrobial Agents and Chemotherapy*, 59(3):1745–1750, 2015. doi: 10.1128/AAC.04435-14.
74. F. E. Nicolás, J. P. de Haro, S. Torres-Martínez, and R. M. Ruiz-Vázquez. Mutants defective in a *Mucor circinelloides dicer*-like gene are not compromised in siRNA silencing but display developmental defects. *Fungal Genetics and Biology*, 44(6):504–516, 2007. doi: 10.1016/j.fgb.2006.09.003.
75. J. Schindelin, I. Arganda-Carreras, E. Frise, V. Kaynig, M. Longair, T. Pietzsch, S. Preibisch, C. Rueden, S. Saalfeld, B. Schmid, J.-Y. Tinevez, D. J. White, V. Hartenstein, K. Eliceiri, P. Tomancak, and A. Cardona. Fiji: an open-source platform for biological-image analysis. *Nature Methods*, 9(7):676–682, 2012. doi: 10.1038/nmeth.2019.
76. C. Camacho, G. Coulouris, V. Avagyan, N. Ma, J. Papadopoulos, K. Bealer, and T. L. Mad-

den. BLAST+: architecture and applications. *BMC Bioinformatics*, 10(1):421, 2009. doi: 10.1186/1471-2105-10-421.

77. T. Jones, N. A. Federspiel, H. Chibana, J. Dungan, S. Kalman, B. B. Magee, G. Newport, Y. R. Thorstenson, N. Agabian, P. T. Magee, R. W. Davis, and S. Scherer. The diploid genome sequence of *Candida albicans*. *Proceedings of the National Academy of Sciences*, 101(19):7329–7334, 2004. doi: 10.1073/pnas.0401648101.
78. Y. Chang, Y. Wang, S. Mondo, S. Ahrendt, W. Andreopoulos, K. Barry, J. Beard, G. L. Benny, S. Blankenship, G. Bonito, C. Cuomo, A. Desiro, K. A. Gervers, H. Hundley, A. Kuo, K. LaButti, B. F. Lang, A. Lipzen, K. O'Donnell, J. Pangilinan, N. Reynolds, L. Sandor, M. E. Smith, A. Tsang, I. V. Grigoriev, J. E. Stajich, and J. W. Spatafora. Evolution of zygomycete secretomes and the origins of terrestrial fungal ecologies. *iScience*, 25(8):104840, 2022. doi: 10.1016/j.isci.2022.104840.
79. G. Janbon, K. L. Ormerod, D. Paulet, E. J. Byrnes, V. Yadav, G. Chatterjee, N. Mullapudi, C.-C. Hon, R. B. Billmyre, F. Brunel, Y.-S. Bahn, W. Chen, Y. Chen, E. W. L. Chow, J.-Y. Coppée, A. Floyd-Averette, C. Gaillardin, K. J. Gerik, J. Goldberg, S. Gonzalez-Hilarion, S. Gujja, J. L. Hamlin, Y.-P. Hsueh, G. Ianiri, S. Jones, C. D. Kodira, L. Kozubowski, W. Lam, M. Marra, L. D. Mesner, P. A. Mieczkowski, F. Moyrand, K. Nielsen, C. Proux, T. Rossignol, J. E. Schein, S. Sun, C. Wollschlaeger, I. A. Wood, Q. Zeng, C. Neuvéglise, C. S. Newlon, J. R. Perfect, J. K. Lodge, A. Idnurm, J. E. Stajich, J. W. Kronstad, K. Sanyal, J. Heitman, J. A. Fraser, C. A. Cuomo, and F. S. Dietrich. Analysis of the genome and transcriptome of *Cryptococcus neoformans* var. *grubii* reveals complex RNA expression and microevolution leading to virulence attenuation. *PLoS Genetics*, 10(4):e1004261, 2014. doi: 10.1371/journal.pgen.1004261.
80. J. Linde, V. Schwartze, U. Binder, C. Lass-Flörl, K. Voigt, and F. Horn. De novo whole-genome sequence and genome annotation of *Lichtheimia ramosa*. *Genome Announcements*, 2(5):e00888–14, 2014. doi: 10.1128/genomeA.00888-14.
81. S. Triana, A. González, R. A. Ohm, H. A. B. Wösten, H. de Cock, S. Restrepo, and A. Celis. Draft genome sequence of the animal and human pathogen *Malassezia pachydermatis* strain CBS 1879. *Genome Announcements*, 3(5):e01197–15, 2015. doi: 10.1128/genomeA.01197-15.
82. A. Lebreton, E. Corre, J.-l. Jany, L. Brillet-Guéguen, C. Pèrez-Arques, V. Garre, M. Monsoor, R. Debuchy, C. Le Meur, E. Coton, G. Barbier, and L. Meslet-Cladière. Comparative genomics applied to *Mucor* species with different lifestyles. *BMC Genomics*, 21(1):135, 2020. doi: 10.1186/s12864-019-6256-2.
83. E. C. H. Chen, E. Morin, D. Beaudet, J. Noel, G. Yildirir, S. Ndikumana, P. Charron, C. St-Onge, J. Giorgi, M. Krüger, T. Marton, J. Ropars, I. V. Grigoriev, M. Hainaut, B. Henrissat, C. Roux, F. Martin, and N. Corradi. High intraspecific genome diversity in the model arbuscular mycorrhizal symbiont *Rhizophagus irregularis*. *New Phytologist*, 220(4):1161–1171, 2018. doi: 10.1111/nph.14989.
84. S. J. Mondo, O. A. Lastovetsky, M. L. Gaspar, N. H. Schwardt, C. C. Barber, R. Riley, H. Sun, I. V. Grigoriev, and T. E. Pawlowska. Bacterial endosymbionts influence host sexuality and reveal reproductive genes of early divergent fungi. *Nature Communications*, 8(1):1843, 2017. doi: 10.1038/s41467-017-02052-8.
85. A. Goffeau, B. G. Barrell, H. Bussey, R. W. Davis, B. Dujon, H. Feldmann, F. Galibert, J. D. Hoheisel, C. Jacq, M. Johnston, E. J. Louis, H. W. Mewes, Y. Murakami, P. Philippsen, H. Tettelin, and S. G. Oliver. Life with 6000 genes. *Science*, 274(5287):546–567, 1996. doi: 10.1126/science.274.5287.546.
86. V. Wood, R. Gwilliam, M.-A. Rajandream, M. Lyne, R. Lyne, A. Stewart, J. Sgouros, N. Peat, J. Hayles, S. Baker, D. Basham, S. Bowman, K. Brooks, D. Brown, S. Brown, T. Chillingworth, C. Churcher, M. Collins, R. Connor, A. Cronin, P. Davis, T. Feltwell, A. Fraser, S. Gentles, A. Goble, N. Hamlin, D. Harris, J. Hidalgo, G. Hodgson, S. Holroyd, T. Hornsby, S. Howarth, E. J. Huckle, S. Hunt, K. Jagels, K. James, L. Jones, M. Jones, S. Leather, S. McDonald, J. McLean, P. Mooney, S. Moule, K. Mungall, L. Murphy, D. Niblett, C. Odell, K. Oliver, S. O'Neil, D. Pearson, M. A. Quail, E. Rabbinowitsch, K. Rutherford, S. Rutter, D. Saunders, K. Seeger, S. Sharp, J. Skelton, M. Simmonds, R. Squares, S. Squares, K. Stevens, K. Taylor, R. G. Taylor, A. Tivey, S. Walsh, T. Warren, S. Whitehead, J. Woodward, G. Volckaert, R. Aert, J. Robben, B. Grymonprez, I. Weltjens, E. Vanstreels, M. Rieger, M. Schäfer, S. Müller-Auer, C. Gabel, M. Fuchs, C. Fritzc, E. Holzer, D. Moestl, H. Hilbert, K. Borzym, I. Langer, A. Beck, H. Lehrach, R. Reinhardt, T. M. Pohl, P. Eger, W. Zimmermann, H. Wedler, R. Wambutt, B. Purnelle, A. Goffeau, E. Cadieu, S. Dréano, S. Gloux, V. Lelaure, S. Mottier, F. Galibert, S. J. Aves, Z. Xiang, C. Hunt, K. Moore, S. M. Hurst, M. Lucas, M. Rochet, C. Gaillardin, V. A. Tallada, A. Garzon, G. Thode, R. R. Daga, L. Cruzado, J. Jimenez, M. Sánchez, F. del Rey, J. Benito, A. Domínguez, J. L. Revuelta, S. Moreno, J. Armstrong, S. L. Forsburg, L. Cerrutti, T. Lowe, W. R. McCombie, I. Paulsen, J. Potashkin, G. V. Shpakovski, D. Ussery, B. G. Barrell, and P. Nurse. The genome sequence of *Schizosaccharomyces pombe*. *Nature*, 415:871–880, 2002. doi: 10.1038/nature724.
87. C. Russ, B. F. Lang, Z. Chen, S. Gujja, T. Shea, Q. Zeng, S. Young, C. A. Cuomo, and C. Nusbaum. Genome sequence of *Spizellomyces punctatus*. *Genome Announcements*, 4 (4):e00849–16, 2016. doi: 10.1128/genomeA.00849-16.
88. S. J. Mondo, R. O. Dannebaum, R. C. Kuo, K. B. Louie, A. J. Bewick, K. LaButti, S. Haridas, A. Kuo, A. Salamov, S. R. Ahrendt, R. Lau, B. P. Bowen, A. Lipzen, W. Sullivan, B. B. Andreopoulos, A. Clum, E. Lindquist, C. Daum, T. R. Northen, G. Kunde-Ramamoorthy, R. J. Schmitz, A. Gryganskyi, D. Culley, J. Magnuson, T. Y. James, M. A. O'Malley, J. E. Stajich, J. W. Spatafora, A. Visel, and I. V. Grigoriev. Widespread adenine N6-methylation of active genes in fungi. *Nature Genetics*, 49(6):964–968, 2017. doi: 10.1038/ng.3859.
89. J. Kämper, R. Kahmann, M. Bölker, L.-J. Ma, T. Brefort, B. J. Saville, F. Banuett, J. W. Kronstad, S. E. Gold, O. Müller, M. H. Perlin, H. A. B. Wösten, R. de Vries, J. Ruiz-Herrera, C. G. Reynaga-Peña, K. Snetselaar, M. McCann, J. Pérez-Martín, M. Feldbrügge, C. W. Basse, G. Steinberg, J. I. Ibeas, W. Holloman, P. Guzman, M. Farman, J. E. Stajich, R. Sentandreu, J. M. González-Prieto, J. C. Kennell, L. Molina, J. Schirawski, A. Mendoza-Mendoza, D. Greilinger, K. Münch, N. Rössel, M. Scherer, M. Vraneš, O. Ladendorf, V. Vincon, U. Fuchs, B. Sandrock, S. Meng, E. C. H. Ho, M. J. Cahill, K. J. Boyce, J. Klose, S. J. Klosterman, H. J. Deelstra, L. Ortiz-Castellanos, W. Li, P. Sanchez-Alonso, P. H. Schreier, I. Häuser-Hahn, M. Vaupel, E. Koopmann, G. Friedrich, H. Voss, T. Schlüter, J. Margolis, D. Platt, C. Swimmer, A. Gnirke, F. Chen, V. Vysotskaia, G. Mannhaupt, U. Güldener, M. Münsterkötter, D. Haase, M. Oesterheld, H.-W. Mewes, E. W. Mauceli, D. DeCaprio, C. M. Wade, J. Butler, S. Young, D. B. Jaffe, S. Calvo, C. Nusbaum, J. Galagan, and B. W. Birren. Insights from the genome of the biotrophic fungal plant pathogen *Ustilago maydis*. *Nature*, 444:97–101, 2006. doi: 10.1038/nature05248.
90. K. Katoh and D. M. Standley. MAFFT multiple sequence alignment software version 7: improvements in performance and usability. *Molecular Biology and Evolution*, 30(4):772–780, 2013. doi: 10.1093/molbev/mst010.
91. S. Capella-Gutierrez, J. M. Silla-Martinez, and T. Gabaldon. trimAl: a tool for automated alignment trimming in large-scale phylogenetic analyses. *Bioinformatics*, 25(15):1972–1973, 2009. doi: 10.1093/bioinformatics/btp348.
92. B. Q. Minh, H. A. Schmidt, O. Chernomor, D. Schrempf, M. D. Woodhams, A. von Haeseler, and R. Lanfear. IQ-TREE 2: new models and efficient methods for phylogenetic inference in the genomic era. *Molecular Biology and Evolution*, 37(5):1530–1534, 2020. doi: 10.1093/molbev/msaa015.
93. A. Dobin and T. R. Gingeras. Mapping RNA-seq Reads with STAR. In *Current Protocols in Bioinformatics*, pages 11.14.1–11.14.19. John Wiley & Sons, Inc., Hoboken, 2015. doi: 10.1002/0471250953.bi1114s51.
94. F. Ramírez, D. P. Ryan, B. Grüning, V. Bhardwaj, F. Kilpert, A. S. Richter, S. Heyne, F. Dündar, and T. Manke. deepTools2: a next generation web server for deep-sequencing data analysis. *Nucleic Acids Research*, 44(W1):W160–W165, 2016. doi: 10.1093/nar/gkw257.
95. H. Tang, J. E. Bowers, X. Wang, R. Ming, M. Alam, and A. H. Paterson. Synteny and collinearity in plant genomes. *Science*, 320(5875):486–488, 2008. doi: 10.1126/science.1153917.
96. L. Lopez-Delisle, L. Rabbani, J. Wolff, V. Bhardwaj, R. Backofen, B. Grüning, F. Ramírez, and T. Manke. pyGenomeTracks: reproducible plots for multivariate genomic datasets. *Bioinformatics*, 37(3):422–423, 2021. doi: 10.1093/bioinformatics/btaa692.
97. J. E. Parker, A. G. S. Warrilow, H. J. Cools, B. A. Fraaije, J. A. Lucas, K. Rigdova, W. J. Griffiths, D. E. Kelly, and S. L. Kelly. Prothioconazole and prothioconazole-desthio activities against *Candida albicans* sterol 14-α-demethylase. *Applied and Environmental Microbiology*, 79(5):1639–45, 2013. doi: 10.1128/AEM.03246-12.

Supplementary information

Table S1

Name	Species	JGI Protein ID	FungiDB Gene ID	EnsemblFungi Gene ID
Erg3	*Candida albicans* SC5314	59490	C1_04770C_A	C1_04770C_A
Erg3	*Choanephora cucurbitarum* NRRL2744	516289		
Erg3	*Cunninghamella echinulata* NRRL1382	185651		
Erg3	*Cryptococcus neoformans* H99	446	CNAG_00519	CNAG_00519
Erg3a	*Lichtheimia corymbifera* JMRC:FSU:9682	10330		LCOR_09389.1
Erg3b	*Lichtheimia corymbifera* JMRC:FSU:9682	4998		LCOR_04579.1
Erg3a	*Lichtheimia ramosa* JMRC:FSU:6197	7192		LRAMOSA02887
Erg3b	*Lichtheimia ramosa* JMRC:FSU:6197	11099		LRAMOSA06288
Erg3	*Malassezia pachydermatis* CBS1879	2056	Malapachy_0912	Malapachy_0912
Erg3	*Mucor circinelloides* 1006PhL	6367	HMPREF1544_06438	HMPREF1544_06438
Erg3	*Mucor lusitanicus* MU402	1381623		
Erg3	*Mucor lusitanicus* CBS277.49 v2.0	156917	QYA_156917	MUCCIDRAFT_156917
Erg3	*Mucor racemosus* UBOCC-A-109155	3973		
Erg3	*Phycomyces blakesleeanus* NRRL1555	178901		
Erg3a	*Rhizopus azygosporus* CBS357.93			CU097_003763
Erg3b	*Rhizopus azygosporus* CBS357.93			CU097_010180
Erg3a	*Rhizopus delemar* 99-880	4689	RO3G_07367	RO3G_07367
Erg3a	*Rhizopus delemar* 99-880	7668	RO3G_13407	RO3G_13407
Erg3	*Rhizopus microsporus* var. *microsporus* ATCC52813	213209		RHIMIDRAFT_213209
Erg3	*Saccharomyces cerevisiae* S288C	4075	YLR056W	YLR056W
Erg31	*Schizosaccharomyces pombe* 972h-	372	SPAC1687.16c	SPAC1687.16c
Erg32	*Schizosaccharomyces pombe* 972h-	2860	SPBC27B12.03c	SPBC27B12.03c
Erg3	*Spizellomyces punctatus* DAOM BR117	5830	SPPG_02338	SPPG_02338
Erg3	*Syncephalastrum racemosum* NRRL2496	499858		
Erg3a	*Sporodiniella umbellata* MES 1446	444990		
Erg3b	*Sporodiniella umbellata* MES 1446	496186		
Erg3	*Ustilago maydis* 521	10884	UMAG_03593	UMAG_03593

Table S1. Erg3 amino acid sequences obtained from the genomes of listed fungal species. Identification numbers from different databases [Joint Genome Institute MycoCosm (JGI, https://mycocosm.jgi.doe.gov), Fungi Database (FungiDB, https://fungidb.org) and Ensembl Fungi (https://fungi.ensembl.org] are indicated to facilitate accessibility and reproducibility.

Table S2

Name	Species	JGI Protein ID	FungiDB Gene ID	EnsemblFungi Gene ID
Erg6	*Candida albicans* SC5314	57503	C3_02150C_A	C3_02150C_A
Erg6a	*Choanephora cucurbitarum* NRRL2744	208609		
Erg6b	*Choanephora cucurbitarum* NRRL2744	449520		
Erg6a	*Cunninghamella echinulata* NRRL1382	280554		
Erg6	*Cryptococcus neoformans* H99	3420	CNAG_03819	CNAG_03819
Erg6a	*Lichtheimia corymbifera* JMRC:FSU:9682	1250		LCOR_01192.1
Erg6b	*Lichtheimia corymbifera* JMRC:FSU:9682	3633		LCOR_03386.1
Erg6d	*Lichtheimia corymbifera* JMRC:FSU:9682	3987		LCOR_03695.1
Erg6a	*Lichtheimia ramosa* JMRC:FSU:6197	1343		LRAMOSA06893
Erg6b	*Lichtheimia ramosa* JMRC:FSU:6197	536		LRAMOSA00533
Erg6d	*Lichtheimia ramosa* JMRC:FSU:6197	2430		LRAMOSA07977
Erg6	*Malassezia pachydermatis* CBS1879	2313	Malapachy_1146	Malapachy_1146
Erg6a	*Mucor circinelloides* 1006PhL	10718	HMPREF1544_10842	HMPREF1544_10842
Erg6b	*Mucor circinelloides* 1006PhL	8587	HMPREF1544_08689	HMPREF1544_08689
Erg6c	*Mucor circinelloides* 1006PhL	9624	HMPREF1544_09736	HMPREF1544_09736
Erg6a	*Mucor lusitanicus* MU402	1319648		
Erg6b	*Mucor lusitanicus* MU402	1325190		
Erg6c	*Mucor lusitanicus* MU402	1448211		
Erg6a	*Mucor lusitanicus* CBS277.49 v2.0	155859	QYA_155859	MUCCIDRAFT_155859
Erg6b	*Mucor lusitanicus* CBS277.49 v2.0	151310	QYA_151310	MUCCIDRAFT_151310
Erg6c	*Mucor lusitanicus* CBS277.49 v2.0	74496	QYA_74496	MUCCIDRAFT_74496
Erg6a	*Mucor racemosus* UBOCC-A-109155	9296		
Erg6b	*Mucor racemosus* UBOCC-A-109155	5625		
Erg6c	*Mucor racemosus* UBOCC-A-109155	11127		
Erg6a	*Phycomyces blakesleeanus* NRRL1555	128748		
Erg6b	*Phycomyces blakesleeanus* NRRL1555	114967		
Erg6a	*Rhizopus azygosporus* CBS357.93			CU097_001869
Erg6a	*Rhizopus delemar* 99-880	9579	RO3G_15767	RO3G_15767
Erg6e	*Rhizopus delemar* 99-880	1008	RO3G_16049	RO3G_16049
Erg6a	*Rhizophagus irregularis* DAOM 197198	1517096		
Erg6b	*Rhizophagus irregularis* DAOM 197198	1668347		
Erg6a	*Rhizopus microsporus* var. *microsporus* ATCC52813	203690		RHIMIDRAFT_203690
Erg6	*Saccharomyces cerevisiae* S288C	4664	YML008C	YML008C
Erg6	*Schizosaccharomyces pombe* 972h-	3100	SPBC16E9.05	SPBC16E9.05
Erg6	*Spizellomyces punctatus* DAOM BR117	8734	SPPG_05059	SPPG_05059
Erg6a	*Syncephalastrum racemosum* NRRL2496	499603		
Erg6b	*Syncephalastrum racemosum* NRRL2496	466111		
Erg6a	*Sporodiniella umbellata* MES 1446	459696		
Erg6e	*Sporodiniella umbellata* MES 1446	469068		
Erg6	*Ustilago maydis* 521	10455	UMAG_03182	UMAG_03182

Table S2. Erg6 amino acid sequences obtained from the genomes of listed fungal species. Identification numbers from different databases [Joint Genome Institute MycoCosm (JGI, https://mycocosm.jgi.doe.gov), Fungi Database (FungiDB, https://fungidb.org) and Ensembl Fungi (https://fungi.ensembl.org] are indicated to facilitate accessibility and reproducibility.

Table S3

Strain	Species	Genotype	Reference
MU402	*M. lusitanicus*	*pyrG*$^-$ *leuA*$^-$	(74)
MU636	*M. lusitanicus*	*pyrG*$^-$::*pyrG*$^+$ *leuA*$^-$	(35)
MIN11	*M. lusitanicus*	*erg3*::*pyrG leuA*-	This study
MIN12	*M. lusitanicus*	*erg3*::*pyrG leuA*-	This study
MIN13	*M. lusitanicus*	*erg6a*::*pyrG leuA*-	This study
MIN14	*M. lusitanicus*	*erg6a*::*pyrG leuA*-	This study
1006PhL	*M. circinelloides*	wildtype	(39)
MIN6	*M. circinelloides*	*pyrF*-59Δ	This study
CPA1	*M. circinelloides*	*pyrF*-59Δ::*pyrF*$^+$	This study
MIN15	*M. circinelloides*	*erg3*::*pyrF*	This study
MIN16	*M. circinelloides*	*erg3*::*pyrF*	This study
MIN17	*M. circinelloides*	*erg6a*::*pyrF*	This study
MIN18	*M. circinelloides*	*erg6a*::*pyrF*	This study

Table S3. Strains used in this study, showing from which species they derive, genotype, and references.

Table S4

Name	Species	Sequence (5' ⟶ 3')	Description
JOHE51488	*Mlu*	TGCCTCAGCATTGGTACTTG	*pyrG* PCR
JOHE51489	*Mlu*	GTACACTGGCCATGCTATCG	*pyrG* PCR
JOHE51528	*Mlu*	CGATAGCATGGCCAGTGTACTAGAGTTTACGATGCAGGCCAGT	*erg3* deletion, overlap with *pyrG*
JOHE51539	*Mlu*	CAAGTACCAATGCTGAGGCAATTTCTGTGTGTCAGTCCGCAC	*erg3* deletion, overlap with *pyrG*
JOHE51529	*Mlu*	ATTAGAACAGAAGGGCAGTCGG	*erg3* deletion
JOHE51538	*Mlu*	CGATCATGCTTACGGTGGTTGAGT	*erg3* deletion
JOHE51540	*Mlu*	CGATAGCATGGCCAGTGTACGTGTGCCAAGTGTAGATGTTGTG	*erg6a* deletion, overlap with *pyrG*
JOHE51552	*Mlu*	CAAGTACCAATGCTGAGGCACATCTGTCTCAATATCCGTCGTC	*erg6a* deletion, overlap with *pyrG*
JOHE51541	*Mlu*	ATTTGCCCGCTGTAGATGATAC	*erg6a* deletion
JOHE51551	*Mlu*	AGTGTAGCAAAAGTTGCCCTTG	*erg6a* deletion
JOHE51511	*Mlu*	ACCTTGAGCACACAAACAAAGG	*pyrG,* 5' junction PCR
JOHE51510	*Mlu*	CCTTTGTTTGTGTGCTCAAGGT	*pyrG,* 3' junction PCR
JOHE51533	*Mlu*	ACAGGAAGTGAGTACAACGGACA	*erg3*, 5' junction PCR
JOHE51534	*Mlu*	CATCGCCTCATACTACTCAAAGC	*erg3*, 3' junction PCR
JOHE51531	*Mlu*	TGTGGTATCTACTGGTTCCATCG	*erg3,* WT allele PCR
JOHE51536	*Mlu*	ATGTTGTGTGTCGAGTAGCACC	*erg3,* WT allele PCR
JOHE51545	*Mlu*	GTCTATGTGGCGCTCAATTCTAC	*erg6a*, 5' junction PCR
JOHE51546	*Mlu*	GCGTCCTCTTCCATTCCTACTAC	*erg6a*, 3' junction PCR
JOHE51543	*Mlu*	GCTGGTGATATTTACGAGTCTGC	*erg6a,* WT allele PCR
JOHE51549	*Mlu*	GGAGAGATTTGATGGTGGTGTT	*erg6a,* WT allele PCR
JOHE51498	*Mci*	AGAATGCCAGACCTGAATTTTTGG	*pyrF* PCR
JOHE51499	*Mci*	AATAGTAATACCCTCTGCCAACGG	*pyrF* PCR
JOHE51623	*Mci*	CCGTTGGCAGAGGGTATTACTATTGATATGGTAGCGAACCCGATG	*erg3* deletion, overlap with *pyrF*
JOHE51628	*Mci*	CCAAAAATTCAGGTCTGGCATTCTAATTTCTGTGTGTCAGTCCGCAC	*erg3* deletion, overlap with *pyrF*
JOHE51624	*Mci*	GGATGAGTCTTCAGGTGCAGTAA	*erg3* deletion
JOHE51627	*Mci*	AATCCGAGAATGATGTGTGAATACC	*erg3* deletion
JOHE51630	*Mci*	CCGTTGGCAGAGGGTATTACTATTCAACATCAAATCTCTCCCGTTC	*erg6a* deletion, overlap with *pyrF*
JOHE51634	*Mci*	CCAAAAATTCAGGTCTGGCATTCTCTCAATATCCGTCTTCCCCTTAC	*erg6a* deletion, overlap with *pyrF*
JOHE51629	*Mci*	AAGATTGGAGCACCTCAAGAGAC	*erg6a* deletion
JOHE51633	*Mci*	AGTCGTGCAGCAGGTAGTTTTAG	*erg6a* deletion
JOHE51503	*Mci*	GAGCAGCAGCATAGAAAGTACCA	*pyrF,* 5' junction PCR
JOHE51504	*Mci*	TATCAAGAAGGACTAGGCTTGCC	*pyrF,* 3' junction PCR
JOHE51625	*Mci*	TGTCACCTACACGAATCTTACCC	*erg3*, 5' junction PCR
JOHE51626	*Mci*	AGAGAATATGGCGCTTCAGAGAC	*erg3*, 3' junction PCR
JOHE51625	*Mci*	TGTCACCTACACGAATCTTACCC	*erg3,* WT allele PCR
JOHE51637	*Mci*	TGTTCATCGGTGGGTTGACG	*erg3,* WT allele PCR
JOHE51631	*Mci*	CTGATTTCACAGTACGCCTGAGT	*erg6a*, 5' junction PCR
JOHE51632	*Mci*	GGTAAAGAATATGGGCACAGGTC	*erg6a*, 3' junction PCR
JOHE51631	*Mci*	CTGATTTCACAGTACGCCTGAGT	*erg6a,* WT allele PCR
JOHE51641	*Mci*	GCATCACCAACATTGGCAAG	*erg6a,* WT allele PCR

Table S4. Species-specific primers [*M. lusitanicus* (*Mlu*) or *M. circinelloides* (*Mci*)] used in this study, showing systematic name, nucleotide sequence, and a brief description explaining its use.

Table S5

Species	Database	Reference
Candida albicans SC5314	JGI	(77)
Choanephora cucurbitarum NRRL2744 v1.0	JGI	(78)
Cryptococcus neoformans var. *grubii* H99	JGI	(79)
Cunninghamella echinulata NRRL1382 v1.0	JGI	(78)
Lichtheimia corymbifera JMRC:FSU:9682	JGI	(45)
Lichtheimia ramosa JMRC:FSU:6197	JGI	(80)
Malassezia pachydermatis CBS1879	JGI	(81)
Mucor circinelloides 1006PhL	JGI	(39)
Mucor lusitanicus MU402 v1.0	JGI	(38)
Mucor racemosus UBOCC-A-109155	JGI	(82)
Phycomyces blakesleeanus NRRL1555 v2.0	JGI	(37)
Rhizophagus irregularis DAOM 197198 v2.0	JGI	(83)
Rhizopus azygosporus CBS357.93	EnsemblFungi	(47)
Rhizopus delemar 99-880	JGI	(46)
Rhizopus microsporus var. *microsporus* ATCC52813 v1.0	JGI	(84)
Saccharomyces cerevisiae S288C	JGI	(85)
Schizosaccharomyces pombe 972h-	JGI	(86)
Spizellomyces punctatus DAOM BR117	JGI	(87)
Sporodiniella umbellata MES 1446 v1.0	JGI	(78)
Syncephalastrum racemosum NRRL2496 v1.0	JGI	(88)
Ustilago maydis 521	JGI	(89)

Table S5. Proteomes from these species were obtained from publicly available repositories either at the Joint Genome Institute MycoCosm (JGI, https://mycocosm.jgi.doe.gov) or, if unavailable, at the EnsemblFungi (https://fungi.ensembl.org) databases.

Figure S1

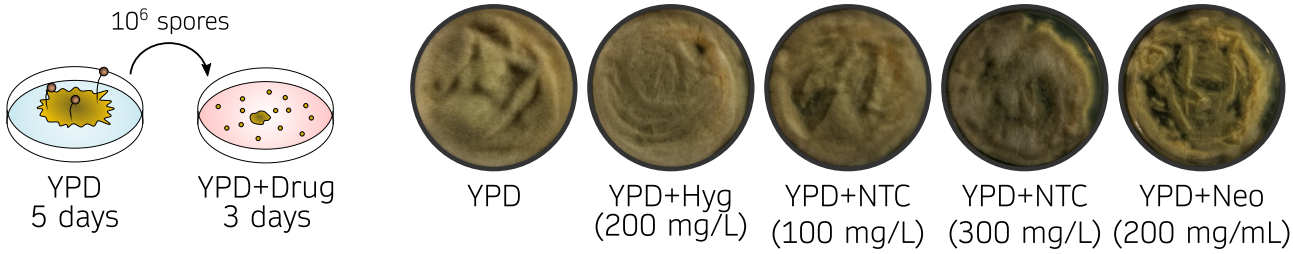

Figure S1. Evaluation of dominant resistance markers in *M. circinelloides*. 10^6 spores from *M. circinelloides* wildtype strain growing for 48 hours on YPD medium supplemented with Hygromycin (Hyg), Nourseothricin (NTC), and Neomycin (Neo) at the indicated concentrations.

Figure S2

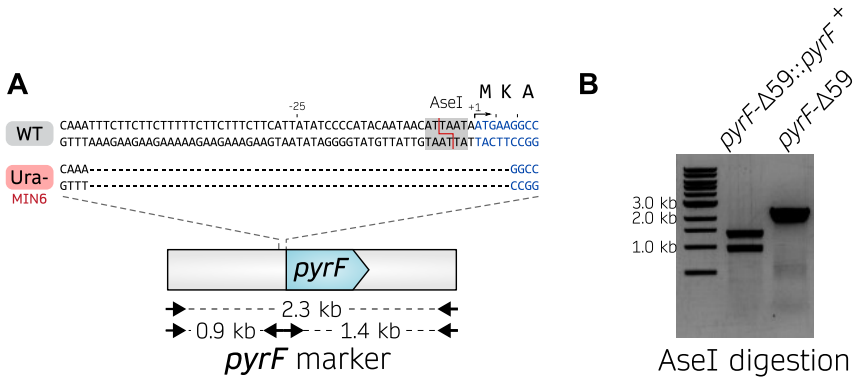

Figure S2. Complementation of the *pyrF* mutant allele in MIN6. (A) Wildtype and MIN6 mutant sequences for *pyrF*. The AseI restriction site is indicated in the wildtype 5' region of the *pyrF* gene, while this restriction site is missing in MIN6. **(B)** PCR-amplification followed by AseI digestion confirming *pyrF* complementation.

Figure S3

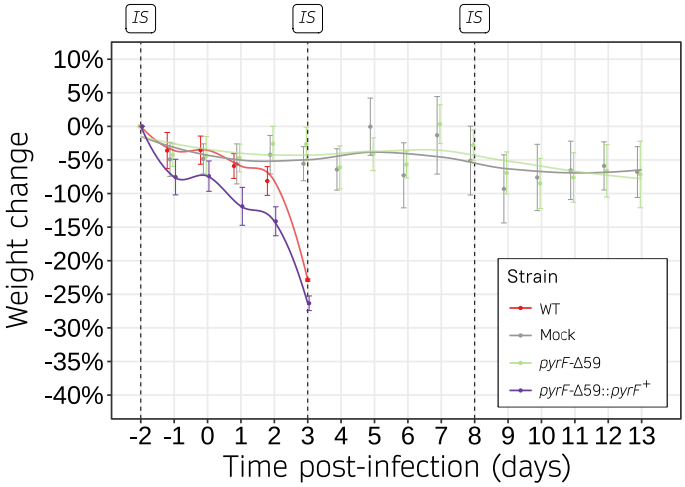

Figure S3. Weight monitoring of mice infected with uracil auxotrophic and prototrophic strains. Body weight of animals infected with wildtype 1006PhL, *pyrF*-59Δ auxotrophic strain, and *pyrF*-59Δ::*pyrF*$^+$ complemented strain. Animals infected with prototrophic strains (red and purple) show increased weight loss over time compared to animals infected with the auxotrophic strain (green) or PBS (gray). Immunosuppressive (IS) treatments are indicated as dotted lines.

Figure S4

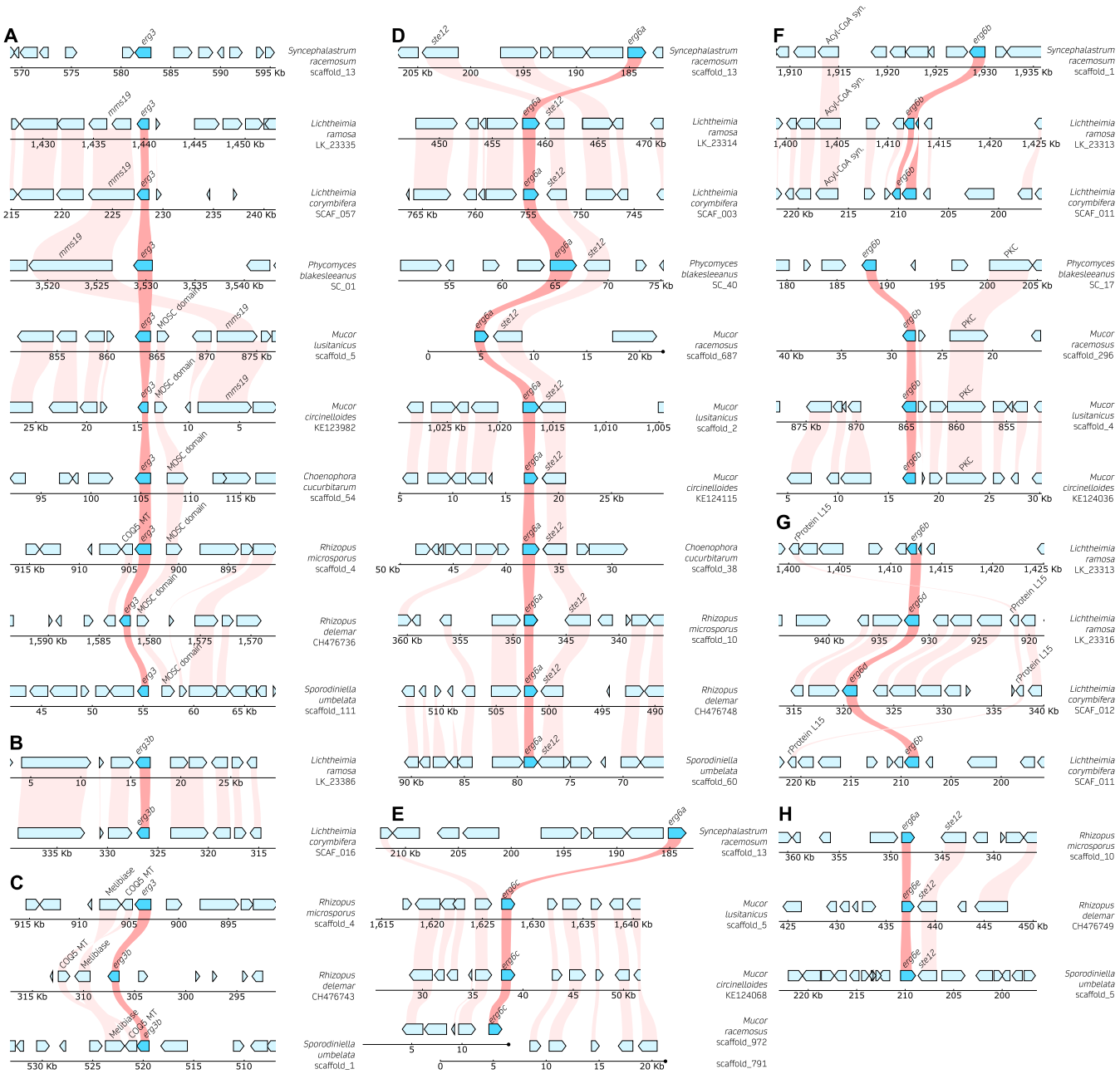

Figure S4. Synteny of *erg3* and *erg6* orthologs within the Mucoromycota. Gene synteny of the indicated species and chromosome locations of genes **(A)** *erg3*, **(B)** *erg3b* in *Lichtheimia* spp., **(C)** *erg3b* in *Rhizopus* spp., **(D)** *erg6a*, **(E)** *erg6c*, **(F)** *erg6b*, **(G)** *erg6d*, and **(H)** *erg6e*. The genome coordinates are indicated for each genome, and gene annotation is depicted as blue blocks highlighting the *erg* genes in cyan blue. Interspecies synteny among genes is depicted as red shading for *erg* genes and as pink shading for neighboring genes.

Figure S5

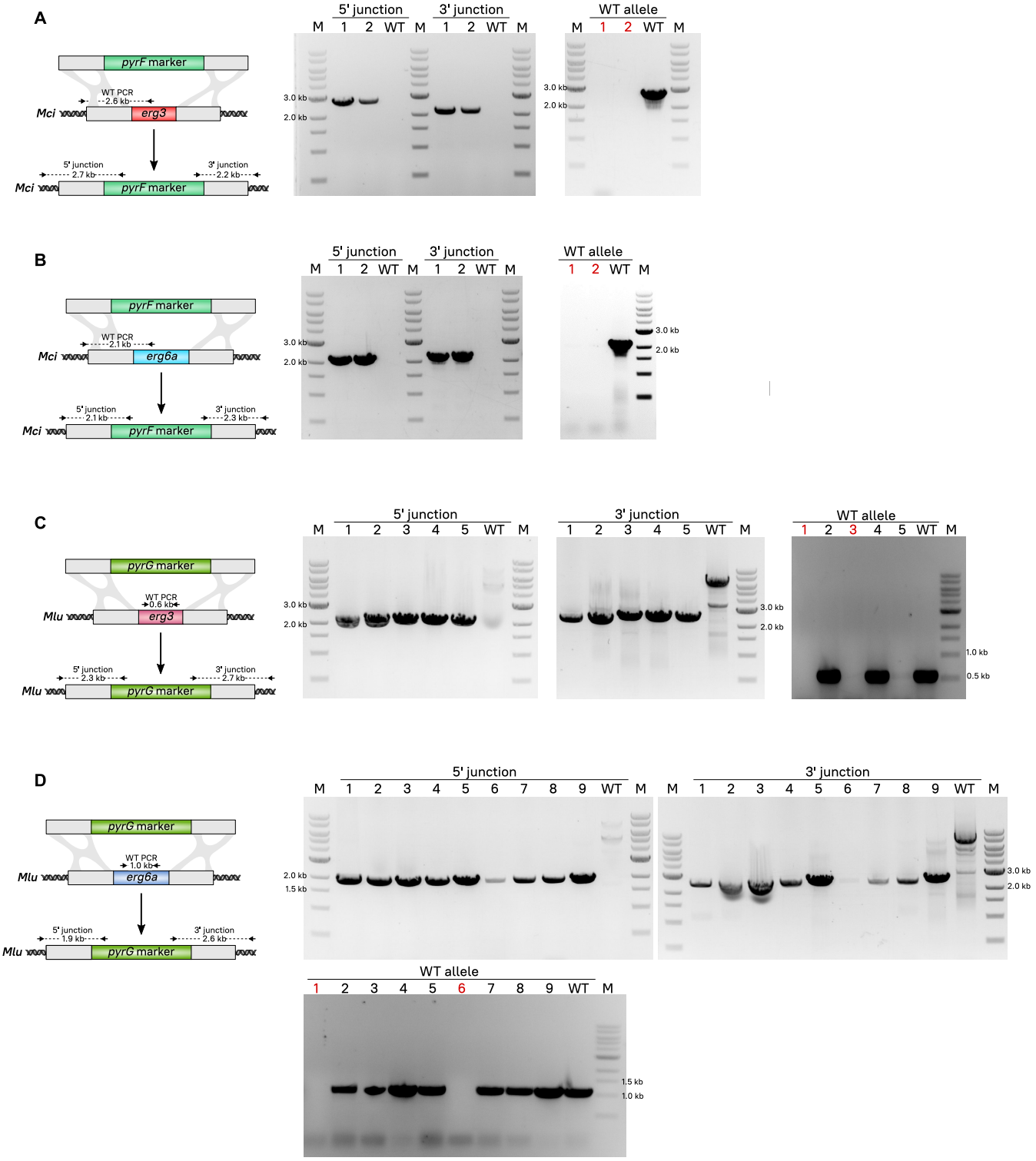

Figure S5. Generation of mutant strains for *erg3* and *erg6a* genes in *M. circinelloides* and *M. lusitanicus*. Diagram (left) and AFLP agarose gel images (right) showing the integration of either the *pyrF* or *pyrG* marker replacing the corresponding *erg* gene: deletion of *erg3* **(A)** and *erg6a* **(B)** in *M. circinelloides*; deletion of *erg3* **(C)** and *erg6a* **(D)** in *M. lusitanicus.* Lanes are numbered to indicate transformant isolates, except for M lanes that show a DNA ladder for fragment size comparison. Arrows mark the annealing regions for specific primers used to confirm the integration by two different PCR reactions: 5' junction, and 3' junction. Mutant homokaryosis was confirmed by absence of the wildtype (WT) allele, and homokaryotic mutants generated by independent transformation experiments are highlighted in red.

Figure S6

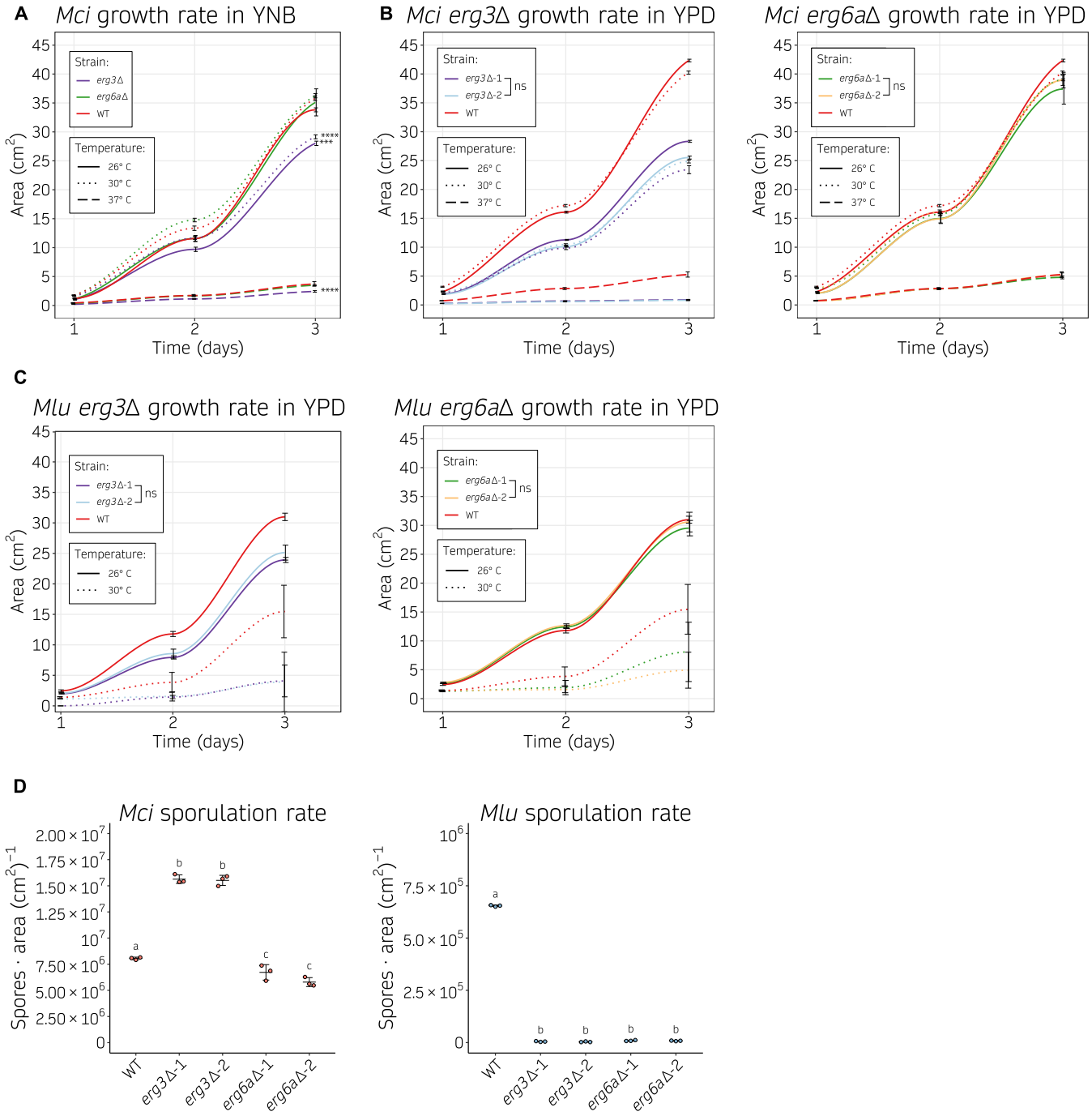

Figure S6. Growth and sporulation rates of *Mucor* species *erg3*Δ and *erg6a*Δ independently generated mutants. (A-C) Growth rate of *Mucor* species strains is depicted as color-coded lines, temperatures are indicated as distinct line types. The growth rate was determined as the area of growth after 24-hour periods. Each experiment was done using six replicates for the wildtype strain (WT), or three biological replicates for each pair of independently generated mutants (Δ-1 and Δ-2) accounting for six total replicates for each deletion and condition tested. Values are plotted as a smoothed curve and SD values as black lines. Growth rate was determined in mutant strains from **(A)** *M. circinelloides* growing in minimal medium YNB; **(B)** *M. circinelloides* rich medium YPD; and **(C)** *M. lusitanicus* in rich medium YPD. One-way ANOVA and Tukey HSD test were conducted for each temperature group and shown as asterisks (** *p-value* $\leq$ 0.01, *** *p-value* $\leq$ 0.001, and **** *p-value* $\leq$ 0.0001) in **(A)**, and to highlight that independently generated mutants harboring the same deletion did not show significant differences (ns) in **(B-C)**. **(D)** Sporulation rate from *M. circinelloides* or *M. lusitanicus* wildtype strains and two *erg3*Δ or *erg6a*Δ independently generated mutants (Δ-1 and Δ-2) was assessed as the number of spores per cm^2 after growing in MMC medium for 48 hours.

Figure S7

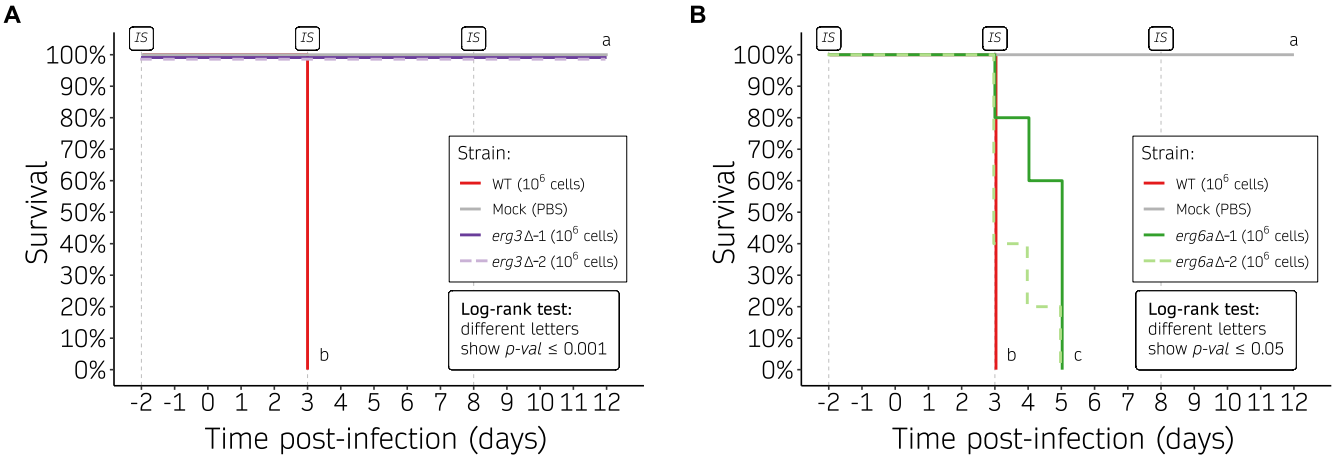

Figure S7. Survival curves of mice infected with *M. circinelloides erg3*Δ and *erg6a*Δ independently generated mutants. Kaplan-Meier survival curves of immunosuppressed mice infected with 10^6 spores from the wildtype strain and either **(A)** *erg3*Δ-1 and *erg3*Δ-2 mutants, or **(B)** *erg6a*Δ-1 and *erg6a*Δ-2. Groups of five mice were inoculated with each independently generated mutant, accounting for ten total mice per deletion or wildtype strain. Strains showing significant differences in virulence assessed by a Log-rank test are indicated as different letters (*p-value* $\leq$ 0.05), confirming that independently generated mutants harboring the same deletion did not show significant differences in virulence. Immunosuppressive treatments are indicated (IS).

Figure S8

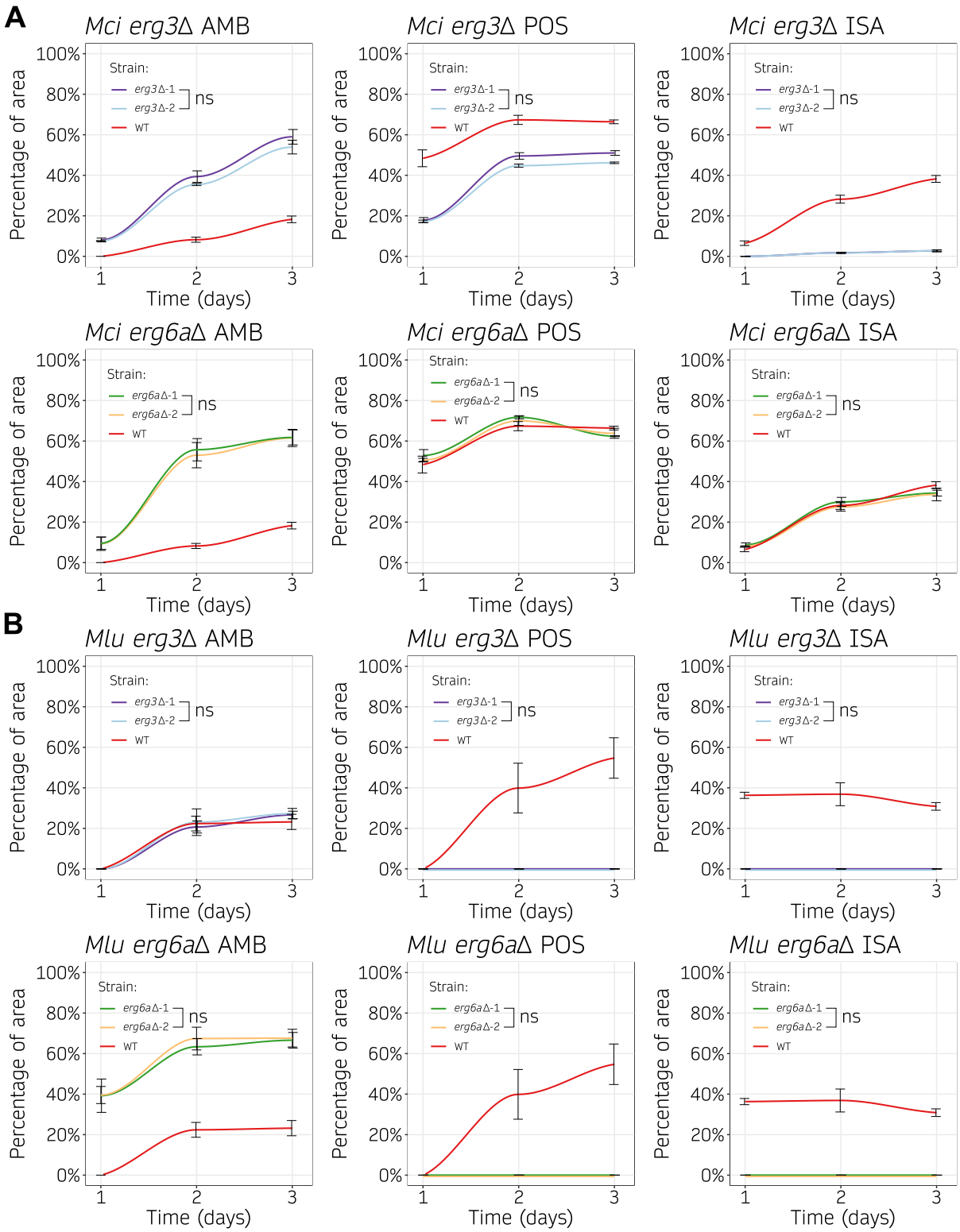

Figure S8. Growth rate during antifungal exposure in *Mucor* species *erg3*Δ and *erg6a*Δ independently generated mutants. Growth across time (24-hour intervals) from independently generated *erg3*Δ and *erg6a*Δ mutants (Δ-1 and Δ-2) in medium containing amphotericin B (AMB, 8 mg/L), posaconazole (POS, 0.2 mg/mL), or isavuconazole (ISA, 8 mg/mL) was determined as the percentage of growth area from the same strain cultured in control medium without drug. Each species was assayed at its optimal temperature, 30 °C and 26 °C for *M. circinelloides* (*Mci*) and *M. lusitanicus* (*Mlu*), respectively. Individual values were collected either in six biological replicates for the wild type or in three biological replicates from each of the two independently generated mutants to plot a color-coded smoothed curve and SD values (black lines). Independently generated mutants exhibiting the same deletion did not show significant differences (ns, One-way ANOVA and Tukey HSD test, p-value ≤ 0.05).

Figure S9

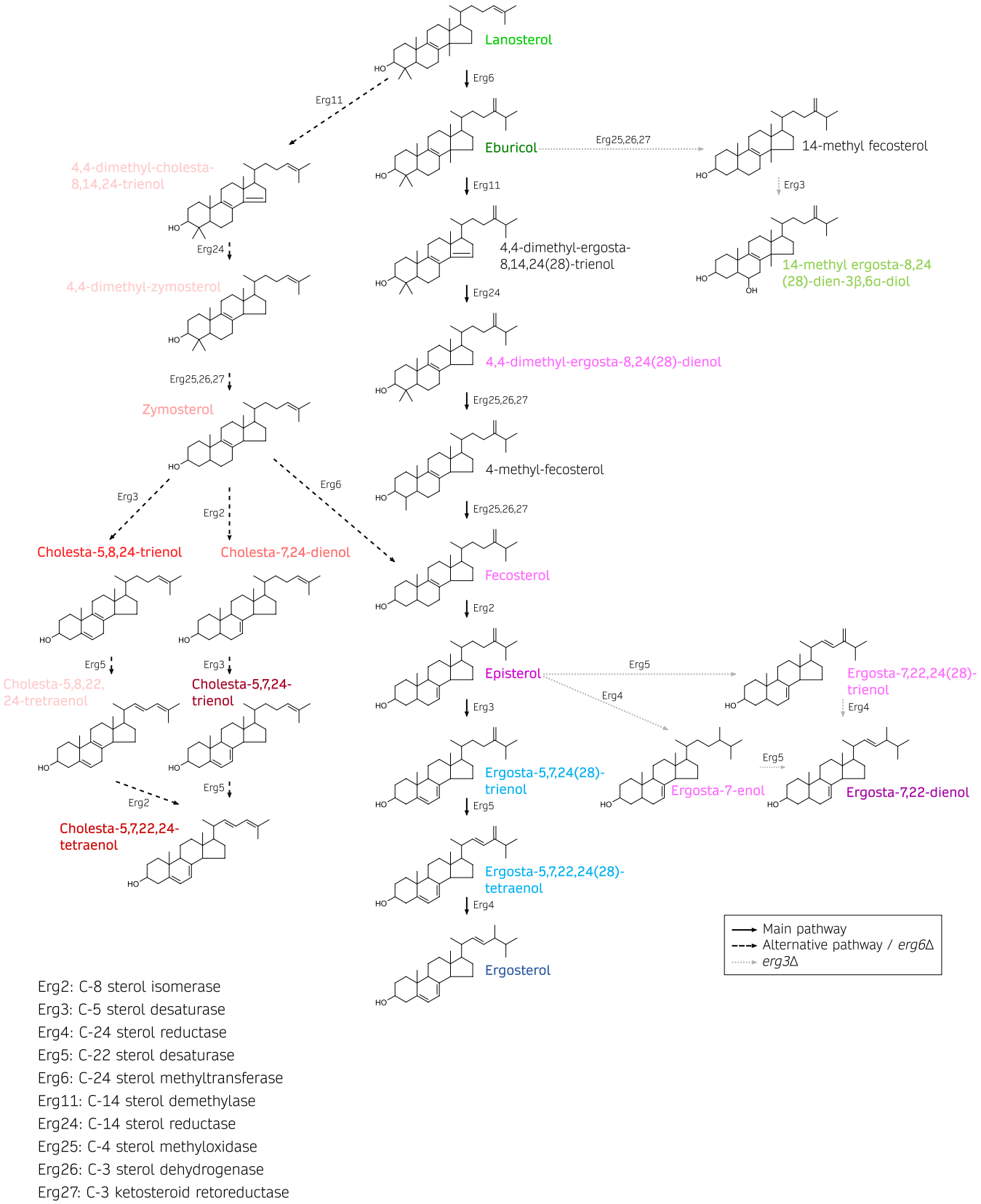

Figure S9. Model of the ergosterol biosynthetic pathway in Mucorales. Pathway schematics showing the compounds (line-angle formula and systematic name) and enzymes (enzymatic activity at bottom legend) comprising the ergosterol biosynthetic pathway in Mucorales. The preferred pathway is depicted by straight, black arrows. Alternative pathways that are relevant in *erg3* (dashed, black arrows) or *erg6a* deletions (dotted, gray arrows) are also shown. For better illustration, sterol compounds are classified and color-coded as in Figure 5A.

Figure S10

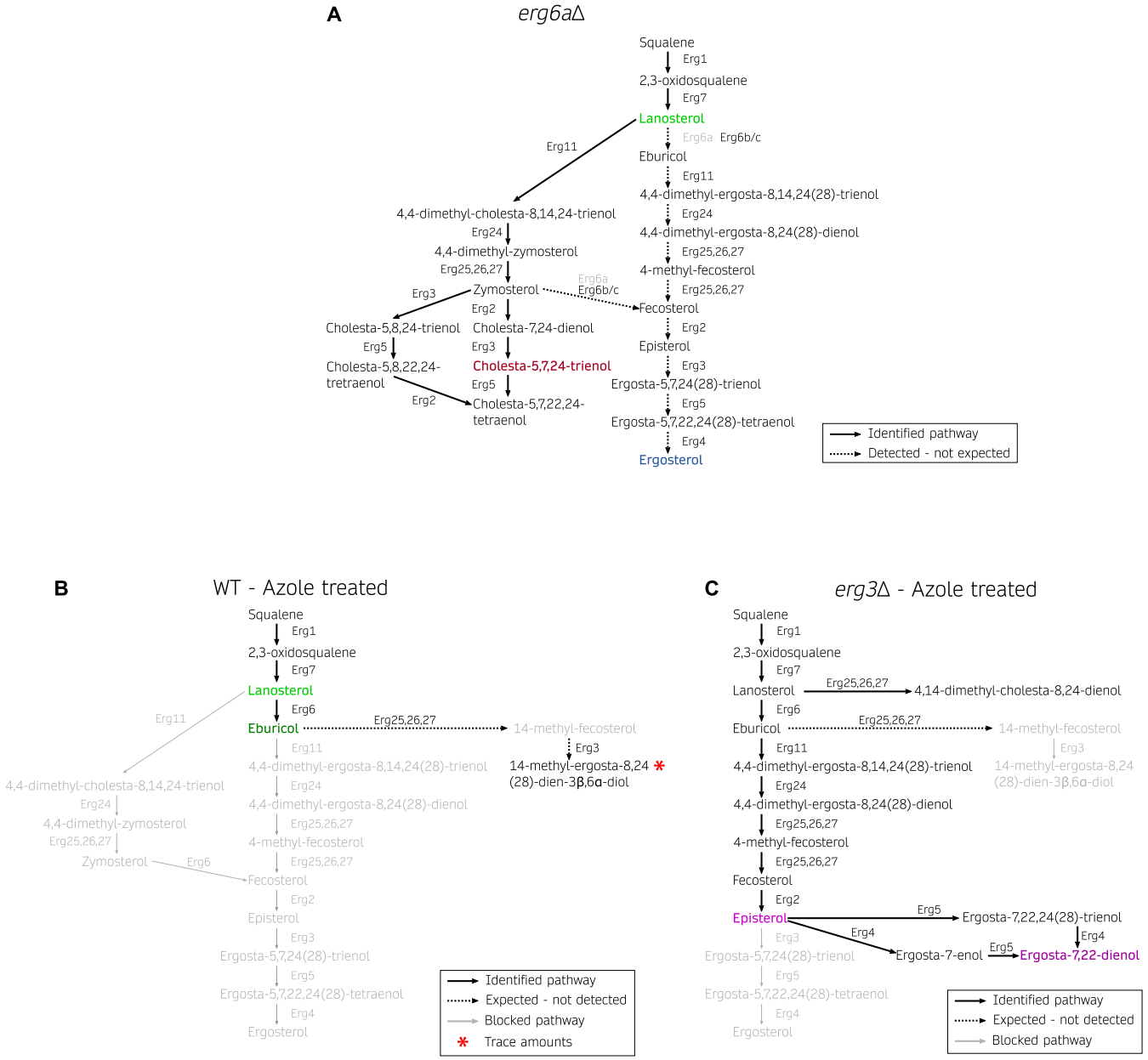

Figure S10. Alternative sterol biosynthetic pathways during azole and amphotericin B treatment in *M. circinelloides*. (A) Cholesta-type sterol accumulation in the *erg6a*Δ mutant with amphotericin B treatment. Erg6a loss-of-function is indicated with gray color, and leads to the accumulation of identified cholesta-type sterols defined by straight, black arrows. Unexpected, residual Erg6 activity was detected by the accumulation of C-24 methylated sterols defined by dashed, black arrows. These sterols, including ergosterol, indicate residual Erg6 activity possibly due to additional Erg6 paralogs, Erg6b or Erg6c. **(B, C)** Accumulation of 14-methylated sterols and other ergosta-type sterols during posaconazole and isavuconazole (azoles) exposure. Identified compounds and reactions are indicated with black arrows, while unidentified compounds and reactions are shown as gray arrows (blocked pathway). Blockades due to azole-mediated Erg11 inhibition in the wildtype strain **(B)** and in *erg3*Δ mutants **(C)** are depicted. Dashed, black arrows indicate the expected accumulation of 14-methyl-fecosterol and the toxic 3,6-diol, but only trace amounts of the toxic 3,6-diol were detected in the wild-type strain during azole treatment. The most abundant sterol compounds in each pathway are color-coded as follows: green (14-methylated sterols), pink (C-5(6)-saturated ergosta-type sterols), red (cholesta-type sterols), and blue (C-5(6)-desaturated ergosta-type sterols).

Figure S11

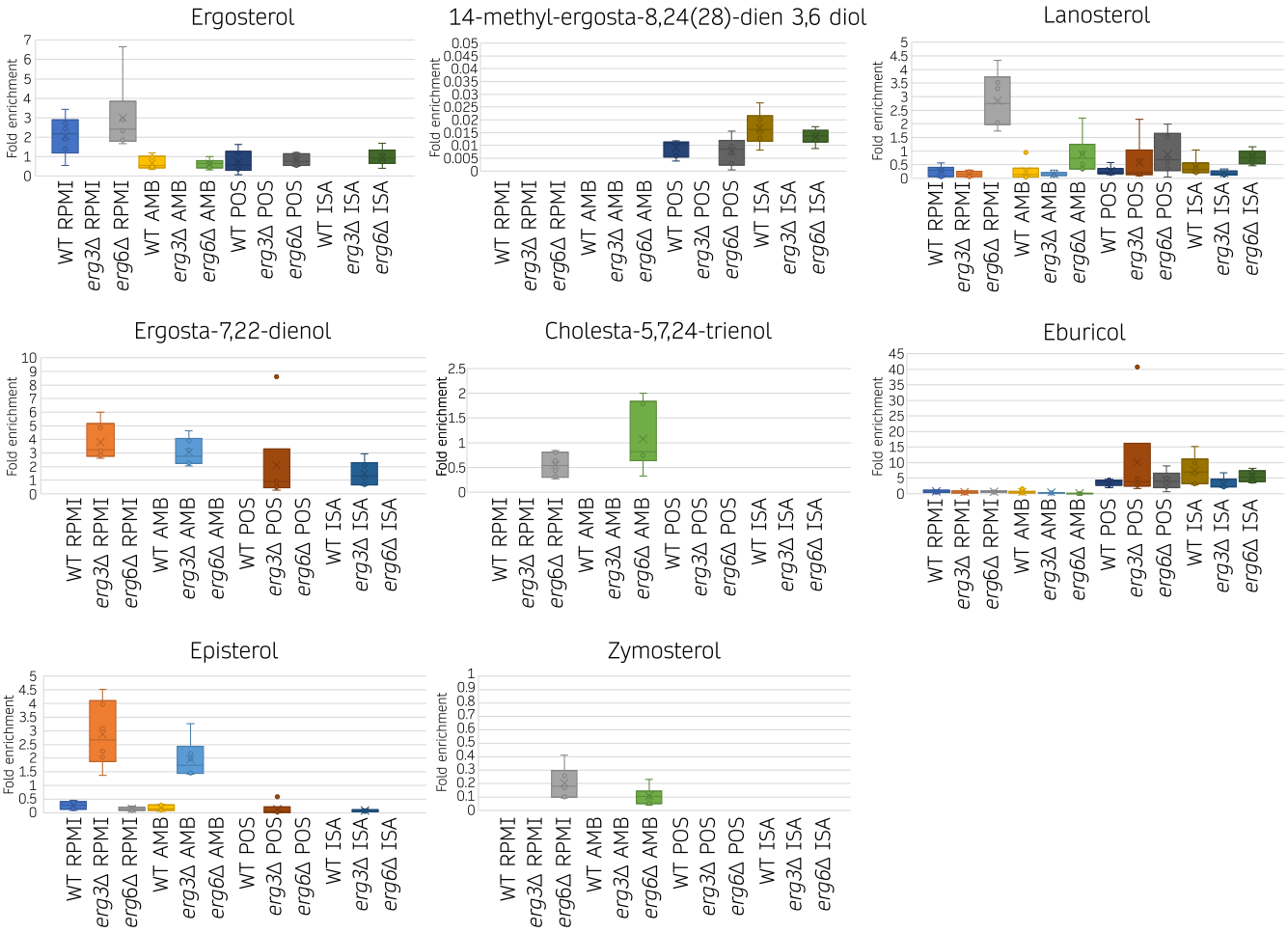

Figure S11. Normalized sterol abundance in *M. circinelloides erg3*Δ and *erg6a*Δ mutants upon amphotericin B and azole treatments. Fold enrichment of different sterols content compared to an internal standard and normalized by the dry weight of each sample. Values were determined from 6 biological replicates, 3 from each pair of independently generated mutant for each deletion, to calculate box plots.

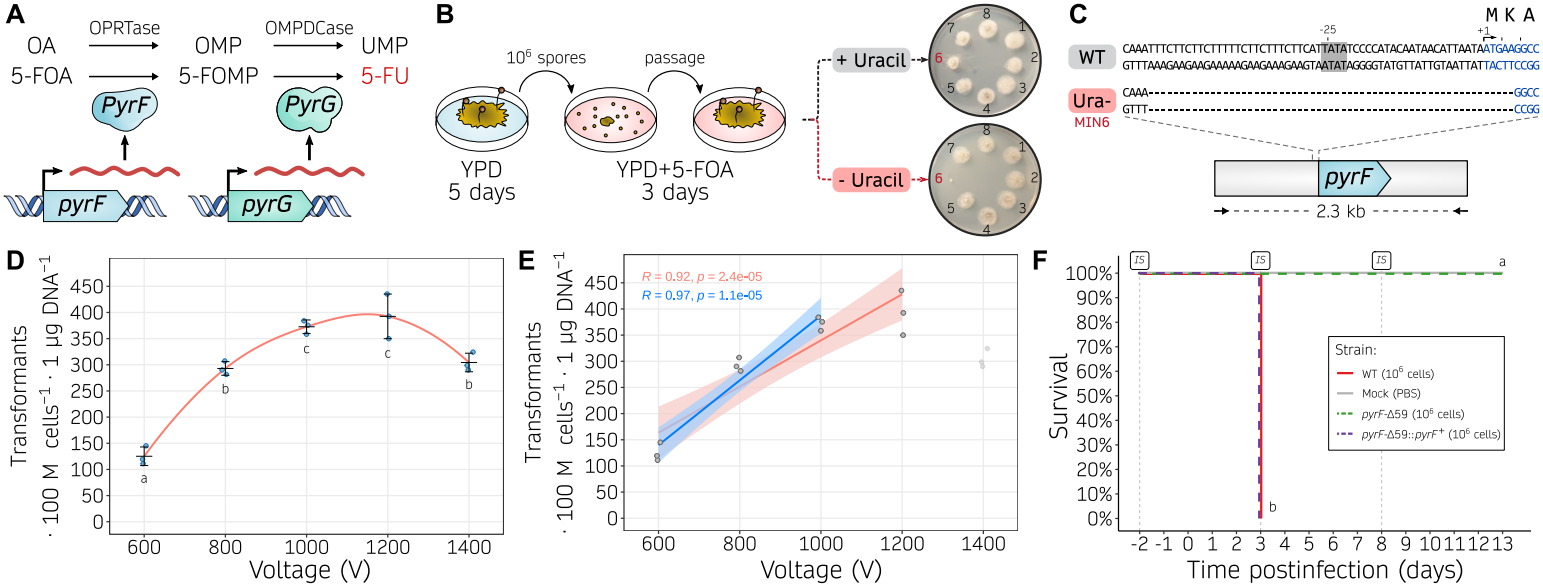
A
OA
5-FOA
OPRTase
OMP
5-FOMP
OMPDCase
UMP
5-FU
PyrF
PyrG
pyrF
pyrG
B
10^6 spores
passage
YPD
5 days
YPD+5-FOA
3 days
+ Uracil
- Uracil
C
M K A
-25
+1
WT
Ura-
MIN6
pyrF
2.3 kb
D
Transformants
· 100 M cells^-1 · 1 µg DNA^-1
Voltage (V)
E
R = 0.92, p = 2.4e-05
R = 0.97, p = 1.1e-05
Transformants
· 100 M cells^-1 · 1 µg DNA^-1
Voltage (V)
F
IS
Survival
Time postinfection (days)
Strain:
WT (10^6 cells)
Mock (PBS)
pyrF-Δ59 (10^6 cells)
pyrF-Δ59::pyrF+ (10^6 cells)

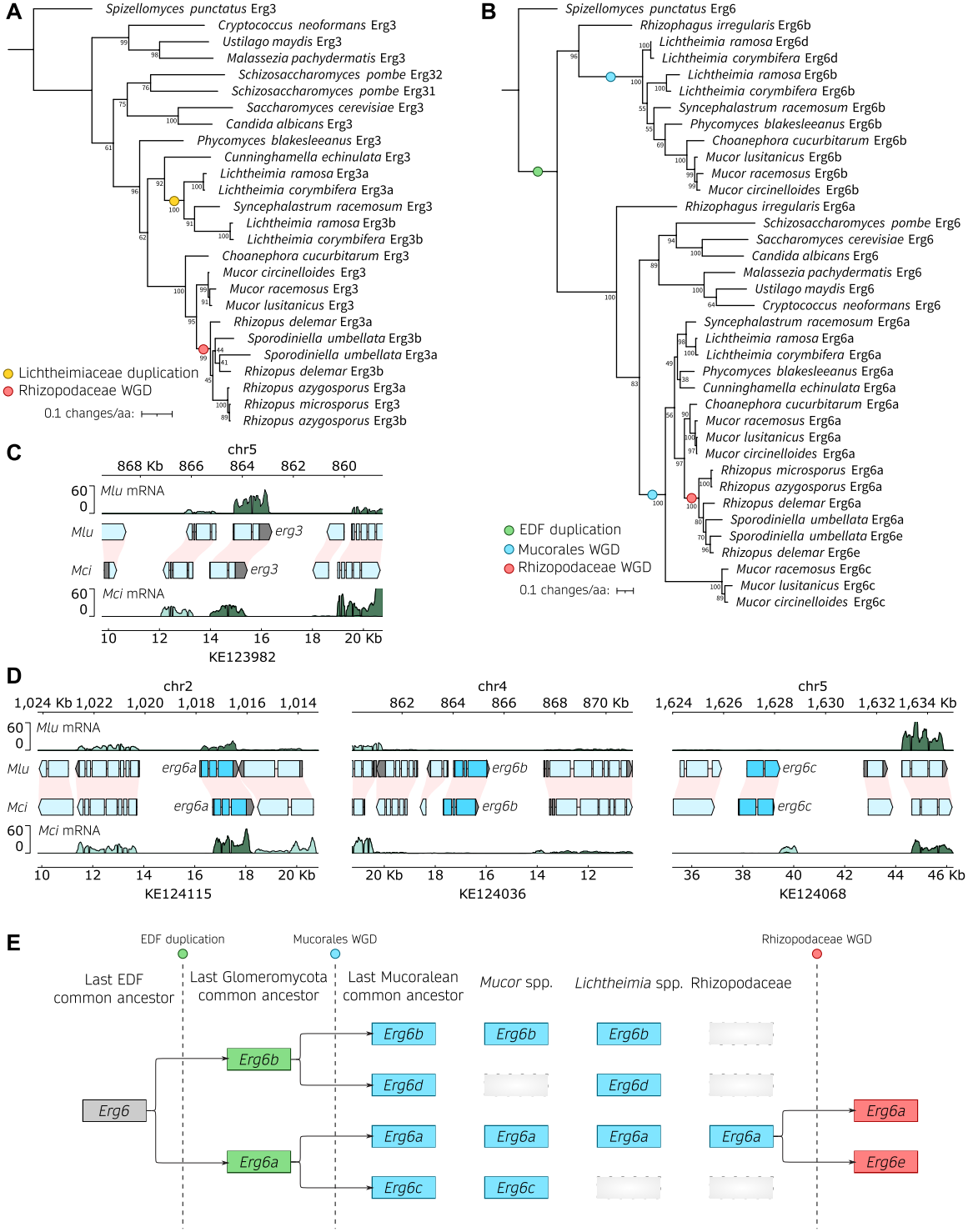
A
Spizellomyces punctatus Erg3
Cryptococcus neoformans Erg3
Ustilago maydis Erg3
Malassezia pachydermatis Erg3
Schizosaccharomyces pombe Erg32
Schizosaccharomyces pombe Erg31
Saccharomyces cerevisiae Erg3
Candida albicans Erg3
Phycomyces blakesleeanus Erg3
Cunninghamella echinulata Erg3
Lichtheimia ramosa Erg3a
Lichtheimia corymbifera Erg3a
Syncephalastrum racemosum Erg3
Lichtheimia ramosa Erg3b
Lichtheimia corymbifera Erg3b
Choanephora cucurbitarum Erg3
Mucor circinelloides Erg3
Mucor racemosus Erg3
Mucor lusitanicus Erg3
Rhizopus delemar Erg3a
Sporodiniella umbellata Erg3b
Sporodiniella umbellata Erg3a
Rhizopus delemar Erg3b
Rhizopus azygosporus Erg3a
Rhizopus microsporus Erg3
Rhizopus azygosporus Erg3b
Lichtheimiaceae duplication
Rhizopodaceae WGD
0.1 changes/aa:
B
Spizellomyces punctatus Erg6
Rhizophagus irregularis Erg6b
Lichtheimia ramosa Erg6d
Lichtheimia corymbifera Erg6d
Lichtheimia ramosa Erg6b
Lichtheimia corymbifera Erg6b
Syncephalastrum racemosum Erg6b
Phycomyces blakesleeanus Erg6b
Choanephora cucurbitarum Erg6b
Mucor lusitanicus Erg6b
Mucor racemosus Erg6b
Mucor circinelloides Erg6b
Rhizophagus irregularis Erg6a
Schizosaccharomyces pombe Erg6
Saccharomyces cerevisiae Erg6
Candida albicans Erg6
Malassezia pachydermatis Erg6
Ustilago maydis Erg6
Cryptococcus neoformans Erg6
Syncephalastrum racemosum Erg6a
Lichtheimia ramosa Erg6a
Lichtheimia corymbifera Erg6a
Phycomyces blakesleeanus Erg6a
Cunninghamella echinulata Erg6a
Choanephora cucurbitarum Erg6a
Mucor racemosus Erg6a
Mucor lusitanicus Erg6a
Mucor circinelloides Erg6a
Rhizopus microsporus Erg6a
Rhizopus azygosporus Erg6a
Rhizopus delemar Erg6a
Sporodiniella umbellata Erg6a
Sporodiniella umbellata Erg6e
Rhizopus delemar Erg6e
Mucor racemosus Erg6c
Mucor lusitanicus Erg6c
Mucor circinelloides Erg6c
EDF duplication
Mucorales WGD
Rhizopodaceae WGD
0.1 changes/aa:
C
chr5
868 Kb 866 864 862 860
Mlu mRNA
Mlu
erg3
Mci
erg3
Mci mRNA
10 12 14 16 18 20 Kb
KE123982
D
chr2
1,024 Kb 1,022 1,020 1,018 1,016 1,014
Mlu mRNA
Mlu
erg6a
Mci
erg6a
Mci mRNA
10 12 14 16 18 20 Kb
KE124115
chr4
862 864 866 868 870 Kb
erg6b
erg6b
20 Kb 18 16 14 12
KE124036
chr5
1,624 1,626 1,628 1,630 1,632 1,634 Kb
erg6c
erg6c
36 38 40 42 44 46 Kb
KE124068
E
EDF duplication
Mucorales WGD
Rhizopodaceae WGD
Last EDF common ancestor
Last Glomeromycota common ancestor
Last Mucoralean common ancestor
Mucor spp.
Lichtheimia spp.
Rhizopodaceae
Erg6
Erg6b
Erg6a
Erg6b
Erg6d
Erg6a
Erg6c
Erg6b
Erg6a
Erg6c
Erg6b
Erg6d
Erg6a
Erg6b
Erg6d
Erg6a
Erg6a
Erg6a
Erg6e

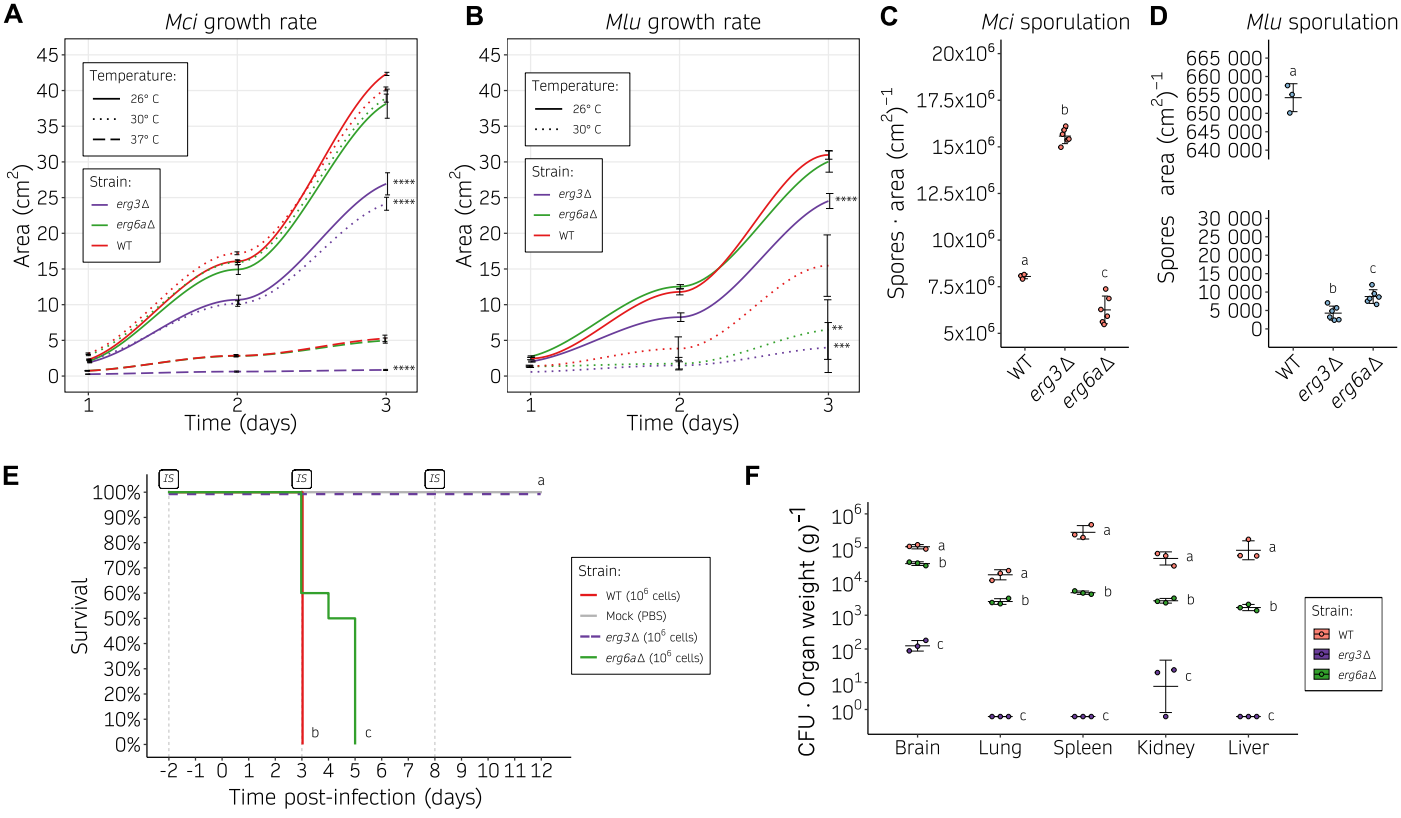
A
Mci growth rate
Temperature:
26° C
30° C
37° C
Strain:
erg3Δ
erg6aΔ
WT
Area (cm2)
Time (days)
B
Mlu growth rate
Temperature:
26° C
30° C
Strain:
erg3Δ
erg6aΔ
WT
Area (cm2)
Time (days)
C
Mci sporulation
Spores · area (cm2)−1
WT
erg3Δ
erg6aΔ
D
Mlu sporulation
Spores · area (cm2)−1
WT
erg3Δ
erg6aΔ
E
IS
Survival
Time post-infection (days)
Strain:
WT (10^6 cells)
Mock (PBS)
erg3Δ (10^6 cells)
erg6aΔ (10^6 cells)
F
CFU · Organ weight (g)−1
Brain
Lung
Spleen
Kidney
Liver
Strain:
WT
erg3Δ
erg6aΔ

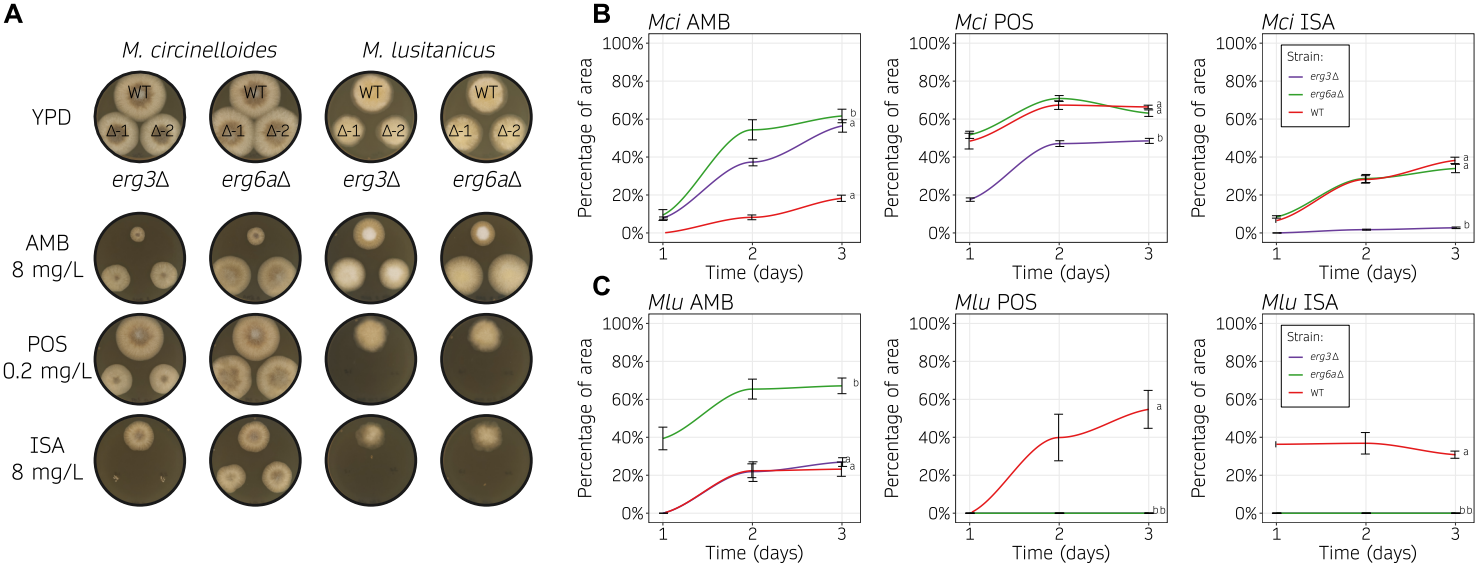
A
M. circinelloides
M. lusitanicus
YPD
WT
Δ-1
Δ-2
erg3Δ
erg6aΔ
AMB
8 mg/L
POS
0.2 mg/L
ISA
8 mg/L
B
Mci AMB
Mci POS
Mci ISA
C
Mlu AMB
Mlu POS
Mlu ISA
Percentage of area
Time (days)
Strain:
erg3Δ
erg6aΔ
WT

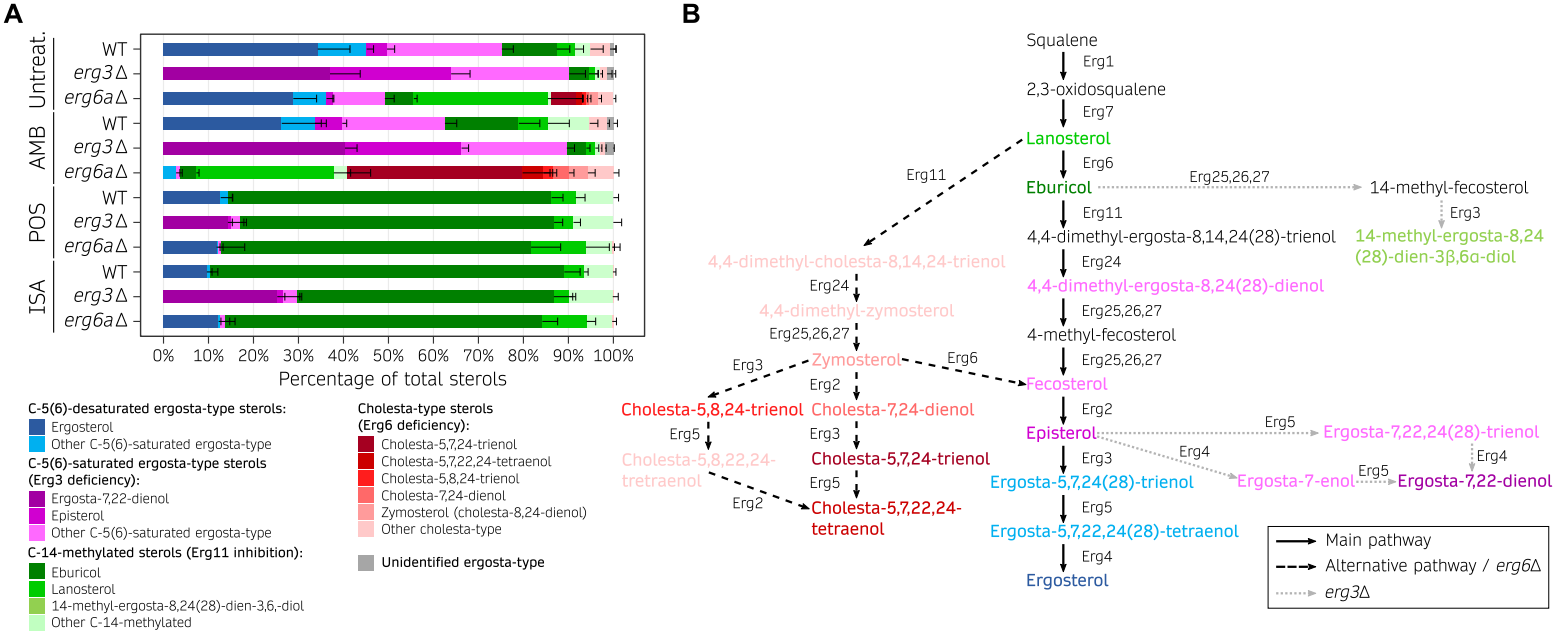
A
Untreat.
AMB
POS
ISA
WT
erg3Δ
erg6aΔ
0%
10%
20%
30%
40%
50%
60%
70%
80%
90%
100%
Percentage of total sterols
C-5(6)-desaturated ergosta-type sterols:
Ergosterol
Other C-5(6)-saturated ergosta-type
C-5(6)-saturated ergosta-type sterols (Erg3 deficiency):
Ergosta-7,22-dienol
Episterol
Other C-5(6)-saturated ergosta-type
C-14-methylated sterols (Erg11 inhibition):
Eburicol
Lanosterol
14-methyl-ergosta-8,24(28)-dien-3,6,-diol
Other C-14-methylated
Cholesta-type sterols (Erg6 deficiency):
Cholesta-5,7,24-trienol
Cholesta-5,7,22,24-tetraenol
Cholesta-5,8,24-trienol
Cholesta-7,24-dienol
Zymosterol (cholesta-8,24-dienol)
Other cholesta-type
Unidentified ergosta-type
B
Squalene
Erg1
2,3-oxidosqualene
Erg7
Lanosterol
Erg6
Eburicol
Erg25,26,27
14-methyl-fecosterol
Erg3
14-methyl-ergosta-8,24(28)-dien-3β,6α-diol
Erg11
4,4-dimethyl-ergosta-8,14,24(28)-trienol
Erg24
4,4-dimethyl-ergosta-8,24(28)-dienol
Erg25,26,27
4-methyl-fecosterol
Erg25,26,27
Fecosterol
Erg2
Episterol
Erg5
Ergosta-7,22,24(28)-trienol
Erg4
Erg3
Ergosta-7-enol
Erg5
Ergosta-7,22-dienol
Erg4
Ergosta-5,7,24(28)-trienol
Erg5
Ergosta-5,7,22,24(28)-tetraenol
Erg4
Ergosterol
Erg11
4,4-dimethyl-cholesta-8,14,24-trienol
Erg24
4,4-dimethyl-zymosterol
Erg25,26,27
Zymosterol
Erg3
Erg6
Cholesta-5,8,24-trienol
Erg5
Cholesta-5,8,22,24-tetraenol
Erg2
Cholesta-7,24-dienol
Erg3
Cholesta-5,7,24-trienol
Erg5
Cholesta-5,7,22,24-tetraenol
Main pathway
Alternative pathway / erg6Δ
erg3Δ